PAPER

Evaluation of fuelling requirements for core density and divertor heat load control in non-stationary phases of the ITER DT 15 MA baseline scenario

IOP Publishing | International Atomic Energy Agency Nuclear Fusion

Nucl. Fusion **60** (2020) 066015 (25pp) https://doi.org/10.1088/1741-4326/ab7c2c

Evaluation of fuelling requirements for core density and divertor heat load control in non-stationary phases of the ITER DT 15 MA baseline scenario

F. Koechl[1,2], R. Ambrosino[3], P. Belo[1], M. Cavinato[4], G. Corrigan[1], L. Garzotti[1], D. Harting [1], A. Kukushkin[5,a], A. Loarte[5], M. Mattei[6], E. Militello-Asp[1], V. Parail[1], M. Romanelli [1], G. Saibene[4] and R. Sartori[4]

[1] Culham Centre for Fusion Energy, Culham Science Centre, Abingdon OX14 3DB, United Kingdom of Great Britain and Northern Ireland
[2] Fusion@ÖAW, Atominstitut, TU Wien, Stadionallee 2, 1020 Vienna, Austria
[3] CREATE, University of Naples 'Federico II', Naples, Italy
[4] Fusion For Energy Joint Undertaking, Josep Pla 2, 08019 Barcelona, Spain
[5] ITER Organization, Route de Vinon-sur-Verdon, CS 90 046, 13067 St Paul Lez Durance Cedex, France
[6] CREATE, University of Campania 'Luigi Vanvitelli', Naples, Italy

E-mail: Florian.Koechl@ukaea.uk

Received 30 September 2019, revised 26 February 2020
Accepted for publication 3 March 2020
Published 5 May 2020

Abstract

To ensure optimal plasma performance at high Q_{fus} for the baseline scenario foreseen for ITER, the fuelling requirements, in particular for non-stationary phases, need to be assessed by means of integrated modelling to address the special additional challenges facing plasma fuelling on ITER. The fuelling scheme needs to be adjusted to ensure robust divertor heat load control, avoiding complete detachment while still maintaining low divertor temperatures and heat fluxes to minimise W sputtering and contamination of the plasma by impurities. At the same time, the core density needs to be controlled to fulfil requirements for: the application of neutral beam heating with acceptable shine-through losses; a robust transition from L-mode to stationary fusion burn; the maximisation of the fusion yield; and a fast reduction in core particle content in the termination phase. Coupled core-edge-SOL transport calculations have been performed, simulating for the first time the entire ITER plasma evolution from just after the X-point formation until the late termination phase. These calculations are being exploited to find the most effective ways of fuelling and heating DT plasmas without exceeding ITER operational limits (e.g. divertor power density). The most efficient ways to fuel ITER with gas and/or pellet injection have been investigated self-consistently with the integrated core + edge + SOL transport suite of codes, JINTRAC, developed at JET (Romanelli *et al* 2014 *Plasma Fusion Res.* **9** 3403023). Our modelling is exploited to study schemes for gas and pellet fuelling for main ion SOL and core density control, respectively, and for impurity seeding by Ne for the control of SOL radiation, that allow ITER to approach $Q_{\mathrm{fus}} \sim 10$, with plasma evolution successfully controlled to respect major operational limits through all transients from the early ramp-up until the late ramp down phase.

Keywords: ITER,
integrated modelling, JINTRAC, fuelling, baseline scenario, impurity seeding, divertor control

(Some figures may appear in colour only in the online journal)

[a] Present addresses: NRC Kurchatov Institute, Kurchatov sq. 1, 123182 Moscow, Russian Federation
NRNU MEPhI, Kashirskoje av. 31, 115409 Moscow, Russian Federation

1. Introduction

Good insights on optimising performance will be essential for helping ITER reach its primary goal of achieving high Q_{fus} (see e.g. [1–3]). In present devices the edge plasma is fairly transparent to gas fuelling, which implies efficient core fuelling even without pellet injection. In contrast, ITER will feature a hot and dense edge plasma and recycled gas and most fuel gas will be ionised in the far scrape-off-layer (SOL) and will not reach the separatrix [4, 5]. Thus, pellet injection, albeit peripheral, will be vital to fuel the ITER core plasma. The density evolution will be key to determining the heating strategy to reach $Q_{\mathrm{fus}} = 10$ H-mode. Here, for the first time, coupled core + edge + SOL transport modelling calculations have been carried out for the ITER 15 MA/5.3 T DT baseline scenario that follow the entire plasma evolution from just after X-point formation until the late current ramp-down phase to find the most effective ways of fuelling and heating DT plasmas without exceeding ITER operational limits: e.g. minimising neutral beam (NB) shine-through, and limiting divertor power fluxes to <10 MWm^{-2}. The most efficient ways to fuel ITER with gas and/or pellet injection have been investigated self-consistently with the integrated core + edge + SOL transport suite of codes, JINTRAC, developed at JET [6], which combines: JETTO/SANCO, a 1.5D core transport solver including impurities [7, 8]; and EDGE2D/EIRENE, a 2D SOL/edge multi-fluid solver, combined with a kinetic Monte Carlo neutral transport code, that includes plasma interactions with the ITER Be wall and W divertor [9, 10]. This study has been performed as part of a broader modelling activity carried out within the framework of an ITER Task Agreement (C19TD51FE) implemented by Fusion for Energy under Grant GRT-502 as summarised in [11].

At a given input power, as the gas rate is increased in the simulations, the core density increases and then saturates [5, 12]. If attempts are made to increase the gas rate beyond saturation, the density builds up in the SOL, due to poor neutral penetration and insufficient power fluxes, and this may lead to completely detached unstable divertor conditions and possibly a MARFE (multifaceted asymmetric radiation from the edge) [13]. It has recently been demonstrated in the experiment, that stable strongly detached regimes can be realised under certain conditions, albeit at reduced edge confinement [14]. Although they could in principle also be foreseen for ITER divertor operation, this option is not considered in the simulations as a conservative approach. There are indications from previous JINTRAC studies that the maximum Greenwald density fraction $n_{\mathrm{e,lin.avg.}}/n_{\mathrm{GW}}$ that can be achieved with gas fuelling alone in the current ramp-up phase of the ITER DT baseline L-mode phase may be limited to $<\sim$30%, depending on the applied heating power (see [15, 16]). Routine use of pellets might then be required in order to reach sufficient density for absorption of NB power with acceptably low shine-through losses. In this paper, JINTRAC simulations are used to explore the range of $n_{\mathrm{e,lin.avg.}}/n_{\mathrm{GW}}$ that can be sustained while respecting all constraints for divertor operation during the current ramp-up phase as function of the applied power and current ramp rate.

In the 15 MA/5.3 T DT baseline plasma, the heat flux at the separatrix P_{sep} only slightly exceeds by a small factor the L-H transition threshold and alpha heating is essential to reach a good quality ELMy H-mode [17]. The density ramp-up after the L-H transition thus requires careful tuning of the particle throughput from gas and pellets to avoid full divertor detachment, while providing enough fuelling to reach the density required for $Q_{\mathrm{fus}} \sim 10$. With the integrated modelling approach presented here, the viability of a heating (33 MW NB + 20 MW ECRH) and fuelling scheme to reach $Q_{\mathrm{fus}} \sim 10$ is investigated, comparing plasma scenarios where the L-H transition occurs during and after the end of the plasma current ramp (at $I_{\mathrm{pl}} = 10$ MA, and $I_{\mathrm{pl}} = 15$ MA, respectively). The question is addressed whether the foreseen divertor control strategies are compatible with given constraints on core fuelling in the transition to a burning plasma at high Q_{fus} [18, 19]. In particular, we assess whether the level of SOL radiation needed to ensure acceptable divertor power fluxes can be established quickly enough by impurity seeding when the (time-averaged) heat flux to the divertor is strongly increased at the start of the ELMy H-mode phase that is associated with a reduction in the increase in thermal energy content, $\mathrm{d}W_{\mathrm{th}}/\mathrm{d}t$.

For the establishment of the ITER baseline scenario, challenges need to be met not only on the path from early ramp-up to stationary burning plasma conditions, but also for the controlled termination of the discharge, considering the back transition to low confinement and the reduction in plasma current [17, 20, 21]. Scenarios have been developed, using JINTRAC simulations, to handle the H-L transition and current ramp-down while simultaneously satisfying all operational constraints to ensure acceptable divertor power flux and keep the divertor plasma thermally stable. Starting from quasi-stationary pellet-fuelled high density H-mode flat-top conditions at $Q_{\mathrm{fus}} \sim 10$ as described in [11, 22], the plasma current ramp-down phase is modelled with the H-L transition occurring at the maximum current ($I_{\mathrm{pl}} = 15$ MA), and part way through the current ramp down (at $I_{\mathrm{pl}} = 10$ MA). Once again, special emphasis is placed on assessing impurity seeding feedback control that must provide a strongly time dependent target level of divertor radiation during transients encountered in the ramp-down phase. In addition, particle exhaust requirements to keep the density below the Greenwald limit throughout the current ramp-down phase are also assessed.

Section 2 provides a short description of simulation settings and model assumptions. This is followed by a detailed description of the core + edge + SOL modelling results and an assessment of fuelling requirements for core density and divertor control for the complete plasma evolution in the 15 MA/5.3 T ITER DT baseline scenario including non-stationary phases. The transition from the early diverted current ramp-up phase to a burning high Q_{fus} regime is described in section 3. Section 4 gives modelling results for the latter part of the discharge, covering the transition from the stationary high Q_{fus} phase through the H-L transition and I_{pl} ramp down. A short summary is provided in section 5.

2. Simulation setup

The modelling of the ITER DT 15 MA/5.3 T baseline in this paper uses similar tools and transport modelling assumptions that have been used in other recent work [5, 11, 15, 16, 22]. They have recently been validated against non-stationary ITER-relevant JET plasma conditions [19, 23].

All JINTRAC simulations discussed in this paper have been carried out modelling the plasma evolution in the core, edge and SOL region including the interaction with PFCs, by combination of the core transport code JETTO + SANCO with the SOL transport code EDGE2D + EIRENE [24]. Transport in the core and edge region is described by solution of transport equations for the safety factor q, the thermal pressure of electrons and ions p_e, p_i, as well as for densities of D and T, n_D, n_T, and a selection of up to two impurity species (He, Be, or Ne densities n_{He}, n_{Be}, n_{Ne}, depending on the scenario phase in consideration). W sputtering and transport has not been taken into account, since the model used would need to be improved, which is the subject of on-going efforts[6].

Neoclassical transport in the core and edge is modelled by NCLASS [25] for main ions and all impurity stages except for Ne, which is described by application of a bundling scheme with five super-stages in SANCO [26]. Anomalous transport is described by the Bohm/gyro-Bohm (BgB) H-mode model [27] together with a collisionality dependent inwards pinch term. Coefficients were adapted in order to match ITER predictions obtained with the gyro-Landau fluid model GLF-23 [28] as described in [5, 29] in the H-mode phases of the discharge, and by the standard Bohm/gyroBohm L-mode model [30, 31] (including an inwards pinch term proportional to $0.5 \cdot D_{i,BgB}$) when the plasma is in L-mode. Impurity reaction cross-sections are evaluated by ADAS [32]. As $P_{net} = P_{in} - dW_{th}/dt$ approaches $P_{L\text{-}H}$ from above, the transport in the ETB is gradually increased by applying a (reducing) suppression factor $\exp(-(P_{net} - P_{L\text{-}H})/(\lambda \cdot P_{L\text{-}H}))$ to the anomalous heat and particle diffusivities within the ETB, $\chi_{e/i,ETB}$, and $D_{i/imp,ETB}$ (see [17]). The parameter λ is chosen such that anomalous transport is almost fully suppressed for $P_{net}/P_{L\text{-}H} > \sim 1.3$–$1.5$ while it remains significant for lower $P_{net}/P_{L\text{-}H}$ mimicking the effect of reduced H-mode confinement in that case in accordance with experimental observations [33]. It should be noted that the core radiation is neglected in the calculation of P_{net}, which for low to moderate impurity contamination may lead to slightly more optimistic predictions for the L-H transition behaviour. $P_{L\text{-}H}$ is prescribed in the simulations by the scaling proposed in [34]. Resistivity and bootstrap current density are calculated by NCLASS. Momentum transport is determined by the momentum source due to NB injection and assuming a Prandtl number equal to one to prescribe the momentum diffusivity.

The effect of sawteeth on the current density and kinetic profiles is described in a time-averaged way by applying the 'Continuous Sawtooth model'. With this model, the time-averaged profile flattening in the core region that would be obtained by applying a discrete sawtooth model is emulated by applying the value of the neoclassical resistivity evaluated at $q \sim 1.0$ in the sawtooth-affected region where $q < 1.0$ and by an increase of the heat and particle diffusivities $\chi_{e/i}$ and $D_{i/imp}$ by $\sim$0.3–0.5 m^2 s^{-1} in that zone. The effect of ELMs is also considered in a time-averaged way using the Continuous ELM model described in [35]. The pedestal width and the maximum achievable pedestal pressure due to MHD constraints are imposed to be in agreement with EPED1 scaling predictions [36, 37]. Due to the requirement of ELM control schemes limiting the energy loss per ELM to $\Delta W_{ELM} < \sim 1$ MJ to ensure an appropriate lifetime of the ITER PFCs, the achievable pedestal pressure may actually remain below the MHD stability limit depending on the ELM control scheme applied (e.g. ELM triggering by pellet injection or vertical oscillations, or the application of 3-D fields) [38, 39]. There are however indications that ELM mitigation schemes can be optimised for operation close to the MHD threshold. For example, modelling studies carried out with the JOREK code have indicated that ELM triggering by pellets at reduced pellet size at a pedestal pressure of $\sim$90% compared to the EPED1 scaling prediction might be envisaged [40]. Although it is important to take means for the optimisation of ELM control techniques for integrated core-edge scenario development into account, this topic is outside the scope of this paper. In the simulations presented here, the implicit assumption is made that a pedestal pressure near or at the MHD threshold can indeed be achieved through ELM control optimisation.

Auxiliary heating by neutral beams is either modelled with PENCIL [41] or, for the case of an early L-H transition presented in section 3.3, with ASCOT [42, 43], while ECRH heat and current sources are determined by a scaling approximation based on GRAY calculations [44].

The plasma is mainly fuelled in the simulations by neutral atoms due to gas puffing and recycling, applying a fixed wall recycling coefficient of 1.0 for D and T, i.e. assuming complete wall saturation and neglecting the impact of both long-term and dynamic fuel retention at the wall [45], although the latter may be sizeable in the initial phase of the discharge and could significantly affect fuelling control requirements. In addition, pellets are injected for core fuelling with particle deposition profiles being modelled by HPI2 [46, 47]. An upper limit of 200 Pa m^3 s^{-1} needs to be taken into account for the total particle throughput [48]. In the simulations, this is done *a posteriori* by verification that the time-averaged total net particle source due to gas puff, pellet injection and NB injection always remains below this limit (neglecting additional throughput requirements for ELM control by pellet pacing).

The magnetic equilibrium is recalculated every $\sim$100 ms with the 2D equilibrium solver ESCO (including the pressure contribution from fast particles). A fixed full bore plasma shape is prescribed that has been derived from free boundary

[6] The implicit assumption is thus made that the ensuing acceptable divertor power fluxes require lower plasma temperatures and this keeps W sputtering rates sufficiently low such that the plasma contamination by W and its impact on plasma conditions remain negligible. We will therefore take the divertor plasma temperature remaining under $\sim$5 eV in the high particle flux divertor plasma region as a proxy for low W sputtering and plasma contamination by this impurity.

calculations with the CREATE-NL code [49]. This has been confirmed to be achievable and sustainable for all plasma current levels and current ramp rates considered in the modelling ($I_{pl} > 3$ MA), provided that (i) the internal plasma inductance remains within the limits for efficient plasma shape and vertical stability control, and (ii) limits in poloidal flux consumption are respected. (For a detailed analysis of plasma shape and stability control with CREATE-NL for the ITER DT 15 MA/5.3 T baseline scenario, see e.g. [1, 50]).

Standard ITER wall and pump structures and assumptions are applied as described in [5]. Parallel heat and particle transport in the SOL is determined by the standard Braginskij model [51], applying electron and ion heat flux free streaming multipliers $\alpha_e = 0.2$ and $\alpha_i = \infty$ [52, 53] and a viscous flux limit as described in [54], and perpendicular transport is prescribed using radially dependent diffusion coefficients and convection velocities as described in [55]. In the near-SOL, the prescribed transport coefficients are set to match the coefficients set by the core-edge transport models at the separatrix. Further away from the separatrix (at $R - R_{sep} > \sim$0/0.5 cm in the outer mid-plane in L-mode/H-mode resp.) the transport coefficients are set to gradually approach prescribed far-SOL values of $\chi_e = \chi_i = 1.0$ m^2 s^{-1}, $D_{D/T} = D_{imp} = 0.3$ m^2 s^{-1} (see [56]). For a sensitivity scan in SOL transport coefficient assumptions see [5, 15]. Cross-field drifts in the SOL are not included in the simulations.

The maximum time step used for the integration of the transport equations in EDGE2D is set to ~1–5 μs. To reduce the required computation time for these CPU-intensive simulations, a partial coupling scheme is applied (see [24]) with user prescribed time intervals of $\Delta t_1 = 15$–20 ms and $\Delta t_2 = 1$ ms for phases when JETTO + SANCO is evolved alone with fixed boundary conditions, and phases when JETTO + SANCO and EDGE2D + EIRENE are coupled and boundary conditions are exchanged at each time step, respectively. A partial coupling correction scheme is applied, in which correction particle source terms are introduced in EDGE2D + EIRENE in the coupled phase to minimise the error in the time-averaged evolution of SOL particle content with respect to an exact fully coupled calculation. The correction terms are estimated from the time history of the SOL particle content. As this error grows with the duration of the non-coupled phase, Δt_1 is automatically reduced by the correction scheme if the correction particle source terms become sizeable. For the description of neutral dynamics, ~10 000 Monte Carlo particles have been used in each EIRENE iteration which is carried out every ~1–30 EDGE2D time steps. EIRENE is run in time-independent mode, assuming that neutral transport is quasi-stationary, which is a reasonable assumption, as the transport time scales of transients in the simulations presented here always exceed the time scale for neutral transport equilibration. Regarding other edge modelling assumptions, the standard EDGE2D + EIRENE plasma-wall interaction models are used.

3. Transition from early current ramp-up phase to burning high Q_{fus} regime

3.1. Current ramp-up

Simulation scans for the ramp-up phase are described in this section, evaluating the operational range in core density and associated DT puff rate requirements, as well as the impact of a variation in auxiliary heating and the current ramp-rate for divertor control and core plasma conditions.

In these simulations, a scenario with early transition from the limiter to divertor configuration is considered, where the plasma is in a diverted configuration for $t > 10$ s, $I_{pl} > 3$ MA. The plasma is fuelled by application of DT gas puff only. Auxiliary heating is provided by ECRH only in this phase, with a maximum applied power of 20 MW. The peak in EC power deposition is located at $\rho_{norm} = 0.2$.

3.1.1. Scan in applied nominal DT gas puff rates. In this scan, the plasma current I_{pl} is linearly ramped up from 3 MA to 15 MA for $t = 10$–80 s. During this period, a constant nominal DT gas puff rate is applied which is updated every 5–15 s. ECRH is applied at a low level of $P_{EC} \sim 5$ MW at $t = 10$ s and then linearly increased to 20 MW at $t = 70$ s. Time traces of I_{pl}, P_{EC}, $n_{e,lin.-avg.}/n_{GW}$ and densities for this scan are shown in figure 1. For all cases, the thermal energy content W_{th} increases from ~2 MJ at the beginning of the ramp to ~17–25 MJ at $I_{pl} = 15$ MA. The internal inductance li(3) is slowly increasing within a range $\sim 0.70 <$ li(3) $< \sim 0.76$ except for the case at low DT gas puff rate $\Gamma_{DT,\,neut} = 3.10^{21}$/s (for which li(3) is decreased to ~0.70 at $I_{pl} = 15$ MA) which is affected by a significant reduction of the inwards diffusion of the edge induced current that is caused by the following causality chain: low $\Gamma_{DT,\,neut} \rightarrow$ lower core density $\rightarrow$ reduced electron-ion heat exchange $\rightarrow$ increased edge electron temperature $\rightarrow$ reduced edge resistivity. To maintain a constant Greenwald density fraction, the DT gas puff rate needs to be increased with plasma current. Due to the curvature pinch term in the BgB model, the core plasma is slightly peaked. The absolute value of the density scales essentially with the density at the separatrix (see figure 1, right), which in turn is determined by the applied DT gas puff rate $\Gamma_{DT,neut}$, the heat flux to the separatrix P_{sep}, the plasma edge impurity composition and the pump efficiency. In these simulations, the impurity content is very low, with $Z_{eff} \sim 1.1$ in the early ramp-up phase and even lower Z_{eff} later on due to enhanced fuelling by DT gas injection. Divertor plasma temperatures can be controlled to avoid any significant release of W by sputtering, without any need for impurity seeding by Ne, and the He ash source due to fusion reactions remains negligible during ramp-up. In this phase the plasma is only contaminated by a small amount of Be that is released at the main chamber wall. As discussed in [5], predictions for the achievable separatrix density are higher at lower Z_{eff} for a given $\Gamma_{DT,neut}$ and input power P_{AUX}. The

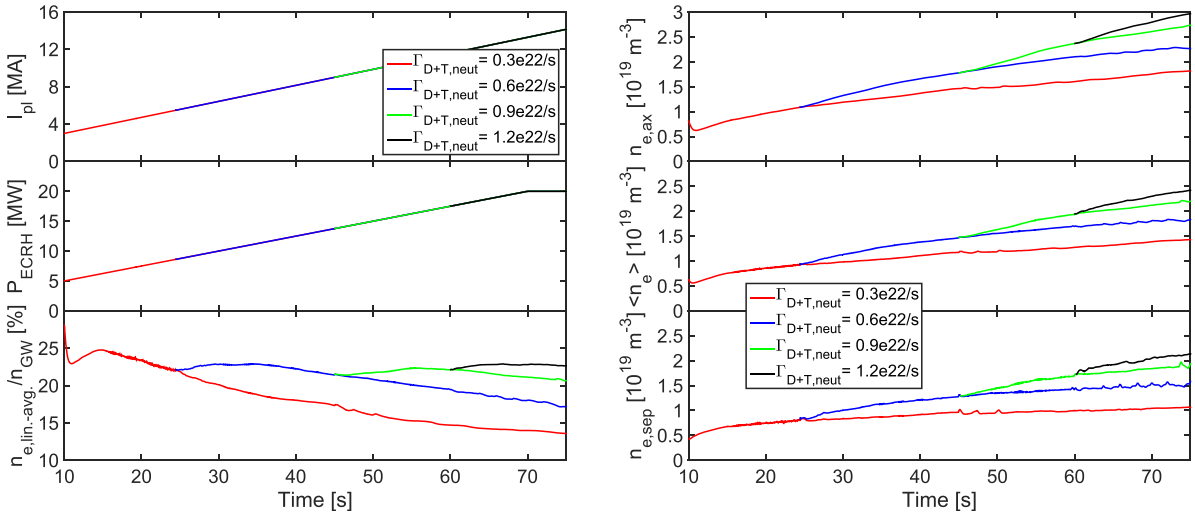

Figure 1. Left, from top to bottom: time evolution of plasma current, EC power and Greenwald density fraction, right: time evolution of central, volume-averaged and separatrix electron density during the current ramp-up from 3 to 15 MA for the scan in nominal DT gas puff rates.

Table 1. Comparison of electron density at the separatrix as predicted by JINTRAC in the current ramp-up scan simulations with scalings derived from SOLPS scans ([57], equations 1 and 3) for varying $\Gamma_{\mathrm{DT,neut}}$ in quasi-stationary conditions at $I_{\mathrm{pl}} = 15$ MA, $P_{\mathrm{AUX}} = 20$ MW, $Z_{\mathrm{eff}} \sim 1.0$.

DT gas puff rate $[10^{22}\ \mathrm{s}^{-1}]$	$n_{\mathrm{e,sep,SOLPS\ scaling}}$ $[10^{19}\ \mathrm{m}^{-3}]$	$n_{\mathrm{e,sep,JINTRAC}}$ $[10^{19}\ \mathrm{m}^{-3}]$	$n_{\mathrm{e,sep,JINTRAC}}/n_{\mathrm{e,sep,SOLPS\ scaling}}$ [%]
0.3	0.66	1.07	162
0.6	1.74	1.55	89
0.9	2.08	1.90	91
1.2	2.19	2.15	98

predictions for n_{sep} obtained by JINTRAC at the end of current ramp-up, when comparable SOL transport conditions are achieved, are in good agreement with recent SOLPS-derived scalings proposed in [57] for a pure gas fuelled plasma (see table 1) except for the case with application of a low DT gas puff rate $\Gamma_{\mathrm{DT,neut}} = 3 \times 10^{21}\ \mathrm{s}^{-1}$ for which a normalised neutral pressure at the entrance of the private flux region $\mu \sim 0.10$ is achieved that appears to lie outside the range of validity of the scalings (see figure 1e in [57]).

The divertor is found to be close to fully detached conditions for the maximum gas puff rates applied in this scan, giving $n_{\mathrm{e,lin.-avg.}}/n_{\mathrm{GW}} \sim 25\%$ (see figure 1, left). This is in agreement with observations from [5, 11, 15] that it may be difficult to increase the density in L-mode to the value $n_{\mathrm{NB,sh.-thr.}}$ that allows unrestricted application of NBI heating with acceptable shine-through loads for DT plasmas by application of gas puff alone. According to [58], the NB shine-through limit in terms of the line-average density along the beam line given as $n_{\mathrm{NB,sh.\ -\ thr.}} \sim 2.3 \times 10^{19}\ \mathrm{m}^{-3}$ is the required density to provide an acceptable power flux on the beryllium first wall panels (specially designed for shine-through power loads of $p_{\mathrm{NB,shine\text{-}through}} < 2\ \mathrm{MWm}^{-2}$) for a 15 MA/5.3 T DT plasma. For a given electron density, the shine-through power fluxes decrease with increasing impurity content. Thus we have taken in our calculation $n_{\mathrm{NB,sh.-thr.}} > 3.0 \times 10^{19}\ \mathrm{m}^{-3}$ to be required for acceptable shine-through losses in the low Z_{eff} plasmas considered in the current ramp up simulations presented here. In our simulations, pellet fuelling is applied to increase the plasma density to the required value before NB heating is applied.

3.1.2. Scan in heating scheme and current ramp rate. In this heating and current ramp-rate scan, a target Greenwald density fraction is prescribed that is maintained by the application of a feedback controlled DT gas puff. The target density fraction is set low enough to avoid strong detachment but still large enough to keep the divertor plasma temperature below ~5 eV on the targets at the location of maximum ion flux in order to avoid a significant release of W. During current ramp-up, the target Greenwald density fraction is adjusted in a stepwise way and kept constant for intervals of ~2–3 MA in terms of the increase in plasma current to achieve an optimal density evolution.

The following three cases have been investigated:

A1. Medium $\mathrm{d}I_{\mathrm{p}}/\mathrm{d}t$, adaptive heating scheme:
- I_{p} linearly ramped from 3 MA to 15 MA between $t = 10$–70 s
- Ohmic heating in early ramp-up phase ($I_{\mathrm{p}} = 3$–5 MA)
- $I_{\mathrm{p}} = 5$–10 MA: linear increase in ECRH power from 0 MW to 20 MW
- $I_{\mathrm{p}} > 10$ MA: 20 MW of ECRH power

A2. Medium $\mathrm{d}I_{\mathrm{p}}/\mathrm{d}t$, linearly increased ECRH power:
- I_{p} linearly ramped from 3 MA to 15 MA between $t = 10$–70 s
- Linear increase in ECRH from 5 MW to 20 MW between $t = 10$–70 s

A3. High $\mathrm{d}I_{\mathrm{p}}/\mathrm{d}t$, linearly increased ECRH power:

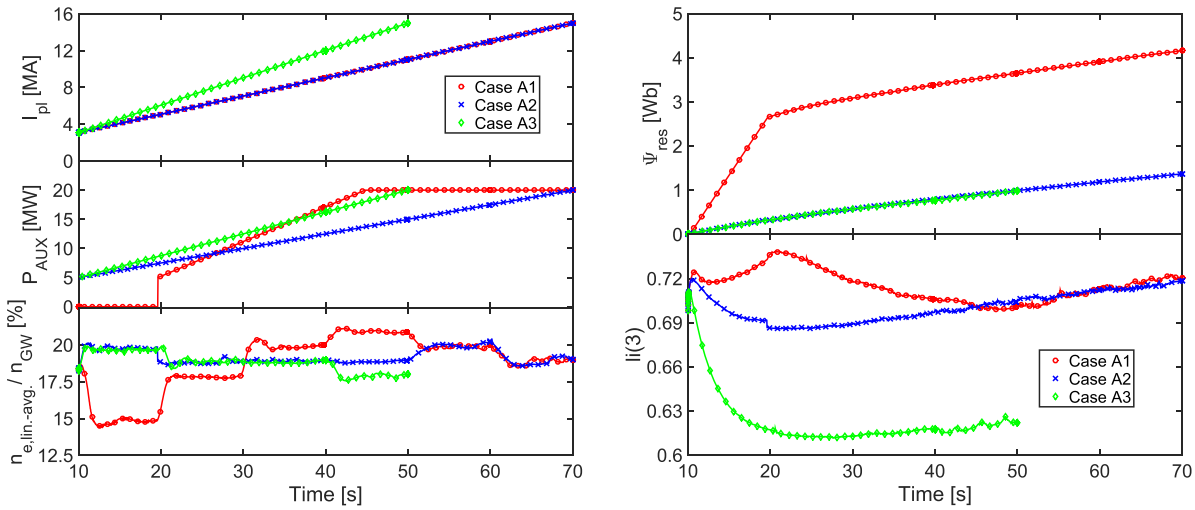

Figure 2. Left: time evolution of plasma current, auxiliary power and Greenwald density fraction (from top to bottom), right: time evolution of resistive poloidal flux consumption (top) and internal inductance li(3) (bottom), during the current ramp-up from 3 to 15 MA for the scan in heating scheme and current ramp rate.

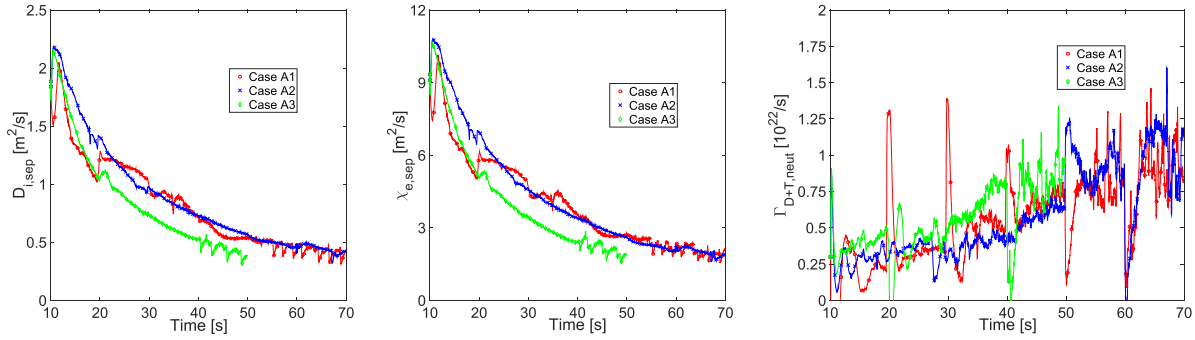

Figure 3. Time evolution of particle (left) and heat diffusivities (middle) at the separatrix and the D + T gas puff rate (right) during the current ramp-up from 3 to 15 MA for the scan in heating scheme and current ramp rate.

- I_p linearly ramped from 3 MA to 15 MA between $t = 10$–50 s
- Linear increase in ECRH from 5 MW to 20 MW between $t = 10$–50 s

The auxiliary heating scheme selected for Case A1 may be representative for typical configurations with purely Ohmic heating at $I_{pl} < \sim 5$ MA and $P_{EC} \sim 20$ MW at $I_{pl} > \sim 10$ MA as considered in previous current ramp-up studies (see [3, 59, 60]). Note that the fastest ramp-up to 15 MA possible in ITER limited by voltages applied and current limits in the superconducting coils is 50 s, while 70 s is a standard ramp-up duration [60].

The plasma evolution for these three cases is shown in figures 2 and 3.

The result above all is that these ramp-up scenarios to $I_{pl} = 15$ MA do not only respect PF coil current limits, but also divertor operational constraints, and can be achieved with the capabilities of the fuelling and heating installed in ITER. Low density operation ($\sim$20% of the Greenwald density limit) with moderate auxiliary heating ($\sim$10 MW) can be achieved in the ramp-up by gas fuelling (see figure 2, left) while avoiding divertor detachment and keeping the plasma temperature at low values in the high particle flux region thus preventing W production. The operational window of achievable densities with gas puff only, explored by variation of the feedback control target for $n_{e,lin\text{-}avg.}/n_{GW}$ in complementary simulations for intervals in I_{pl} of $\sim$2–3 MA, is quite narrow for a given level of P_{AUX} ($\pm \sim 5\%$ of the Greenwald density) so that pellet fuelling is required if larger density variations are required. In our simulation results, gas puff rates are increased by a factor of $\sim$4 when I_{pl} is ramped up from 3 MA to 15 MA to maintain a constant Greenwald density fraction of $\sim$20% (see figure 2, left, figure 3, right). In absolute values, the required DT puff rates vary from 0.25–$1.0 \cdot 10^{22}$ s^{-1} (see figure 3) in this current ramp-up modelling. It should be noted, however, that predictions of the achievable density range by gas puff only depend on SOL transport assumptions as demonstrated e.g. in [5, 15], and thus our results are obtained for the specific assumptions as described in section 2.

The achievable densities are very low for Ohmically heated plasmas ($<\sim$15% of n_{GW}) at low currents, as shown in figure 2, left for the initial phase of Case A1. Low I_{pl} plasmas have a large perpendicular diffusion coefficient because of the high safety factor (see figure 3, left) according to the Bohm/gyro-Bohm model that we use for L-mode modelling.

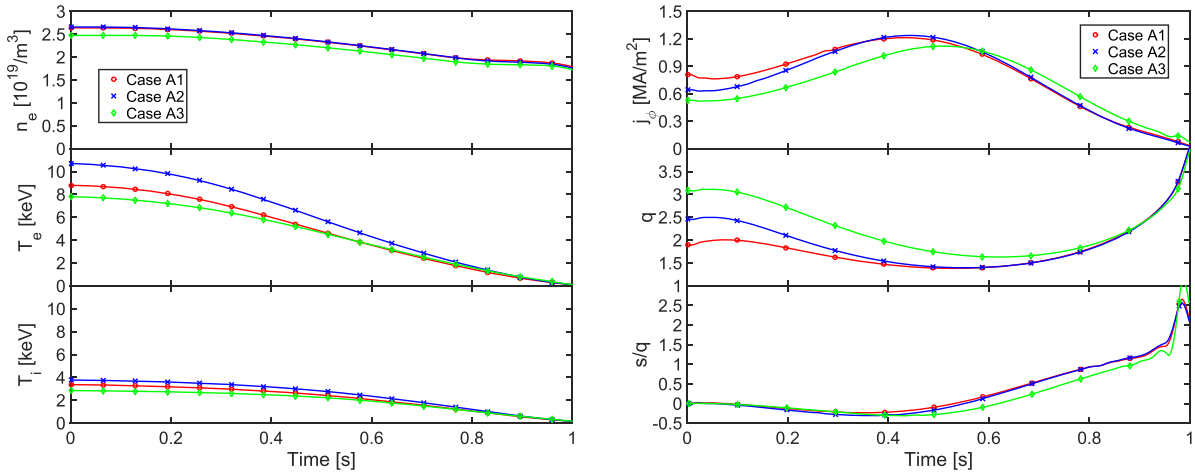

Figure 4. Final plasma profiles when the current has reached 15 MA for current ramp-up from 3 to 15 MA for the scan in heating scheme and current ramp rate. Left, from top to bottom: electron density, electron temperature, ion temperature. Right, from top to bottom: toroidal current density, safety factor, ratio between magnetic shear and safety factor.

This together with the long connection length leads to a wide SOL power fall-off length and detachment to set in already at very low densities. Therefore, a moderate level of heating in the ramp-up ($P_{\mathrm{AUX}} \geq \sim$10 MW) is required both to maintain an appropriate level of plasma density in this phase as well as to reduce the resistive poloidal flux losses that may limit the burn duration in the flat-top phase at 15 MA (see [1, 61]). Resistive losses increase by ∼0.25 Wb s^{-1} in Ohmic plasmas compared to those with ∼10 MW heating (see figure 2, right).

Operation at low density during current ramp-up with EC heating has a noticeable impact on current diffusion, as the resistivity is comparably low in these conditions due to the high electron temperatures. This is due to the low thermal coupling between electrons and ions in the core plasma resulting from the low density and the EC power being absorbed exclusively by the electrons (see figure 4, left). This low resistivity leads to the current density profile to remain hollow at the end of ramp-up at $I_{\mathrm{pl}} = 15$ MA (see figure 4, right) even for cases with moderate current ramp rates (i.e. for a total ramp duration of ∼70–80 s). These hollow profiles have low s/q and this may be unfavourable for plasma confinement in the subsequent early burn phase of the discharge as identified in [1].

Increasing the current ramp rate dI_{pl}/dt (Case A3) leads to a modest reduction in flux consumption compared to lower ramp rates dI_{pl}/dt (Case A2), due to the shorter duration of the ramp (see figure 2, right). However, this causes the current profile to be even more hollow at the end of the ramp-up (see figure 4, right), and thus having lower s/q, which may affect the subsequently achievable confinement. Similarly, the internal inductance li(3) is significantly reduced and approaches li(3) ∼0.6 for which plasma shape control by the PF coil currents approaches its limits at 15 MA [50] (see figure 2, right). Regarding fuelling, for the ramp rates in the range explored, no major differences have been identified to achieve similar densities.

3.2. L-H transition and density control to achieve $Q_{fus} \sim 10$ at 15 MA

In the following, modelling investigations are presented with the aim to verify strategies, most notably with respect to divertor control constraints, for the optimum increase of the core density after an L-H transition at $I_{\mathrm{pl}} = 15$ MA to reach a stationary burning regime at $Q_{\mathrm{fus}} \sim 10$ while $P_{\mathrm{net}}/P_{\mathrm{L\text{-}H}}$ may initially remain close to 1.0. Ne seeding requirements and possible challenges for plasma impurity control in the presence of this transient phase are addressed.

The current ramp-up simulation Case A1 as described in section 3.1.2 has been continued for the early flat-top phase at $I_{\mathrm{pl}} = 15$ MA. The simulation is restarted to allow for a different impurity configuration, switching from Be to He and (bundled) Ne. As the density is near the NB shine-through limit of $n_{\mathrm{NB,sh.\,-\,thr.}} \sim 2.3 \times 10^{19}$ m^{-3} [58] at the end of current ramp-up (see figure 4, left), small pellets (with radius $r_{\mathrm{p}} = 2$ mm for spherical shape, corresponding to $N_{\mathrm{p}} \sim 2.1 \cdot 10^{21}$ particles per pellet) are injected at a frequency of ∼5 Hz until a line-average density of $n_{\mathrm{e,lin.\text{-}avg.}} \sim 3 \cdot 10^{19}$ m^{-3} is obtained, which allows unrestricted heating by NBI. Full NBI power of 33 MW is then applied (modelled by PENCIL) and the transition to H-mode is triggered. The density is then maintained at an approximately constant level to ensure a fast increase in pedestal pressure and in central ion temperature such that the net heat flux can be kept above the L-H transition power threshold due to the increase in alpha heating as described in [18, 19]. After a few seconds, the density is then gradually ramped by standard ITER fuelling size pellets ($r_{\mathrm{p}} = 2.86$ mm, $N_{\mathrm{p}} \sim 6.1 \cdot 10^{21}$), or by pellets with reduced size ($r_{\mathrm{p}} = 1.8$–2.27 mm, $N_{\mathrm{p}} \sim 1.5$–$3.0 \cdot 10^{21}$) in the attempt to mitigate pellet-triggered transient perturbations in divertor conditions, to a target density of $n_{\mathrm{e,lin.avg}} \sim 10^{20}$/m^3 using pellet injection feedback control (reaching maximum injection frequencies of ∼4–5 Hz) to reach a stationary H-mode in the burning regime at $Q_{\mathrm{fus}} \sim 10$. To ensure that heat flux densities to the divertor remain below

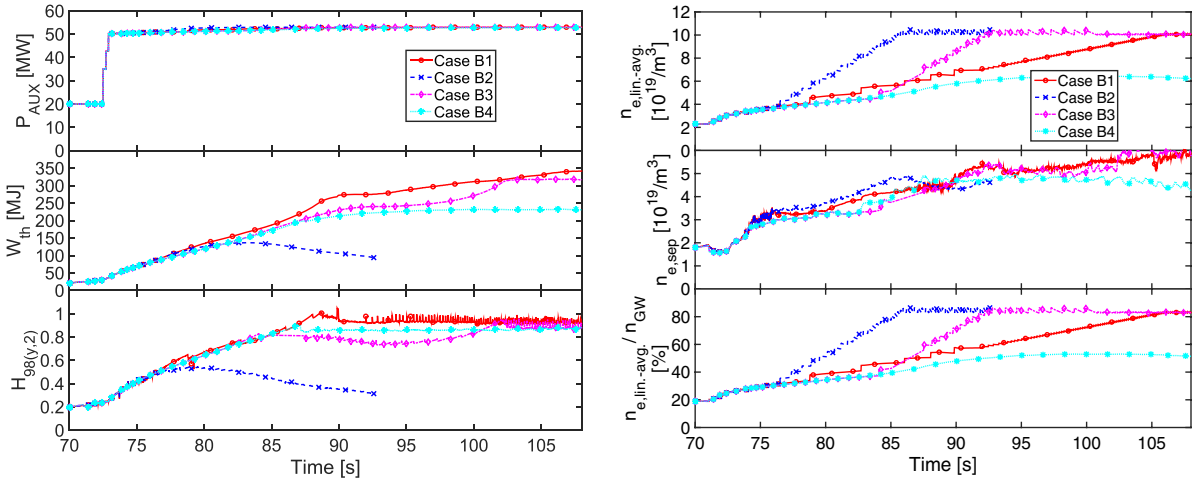

Figure 5. Left: time evolution of auxiliary power, thermal energy content and $H_{(98,y2)}$ factor, right: time evolution of line-averaged electron density, electron density at the separatrix and $n_{e,lin.-avg.}/n_{GW}$ (from top to bottom), from the end of ramp-up at 15 MA, for Cases B1–B4 as described in section 3.2.

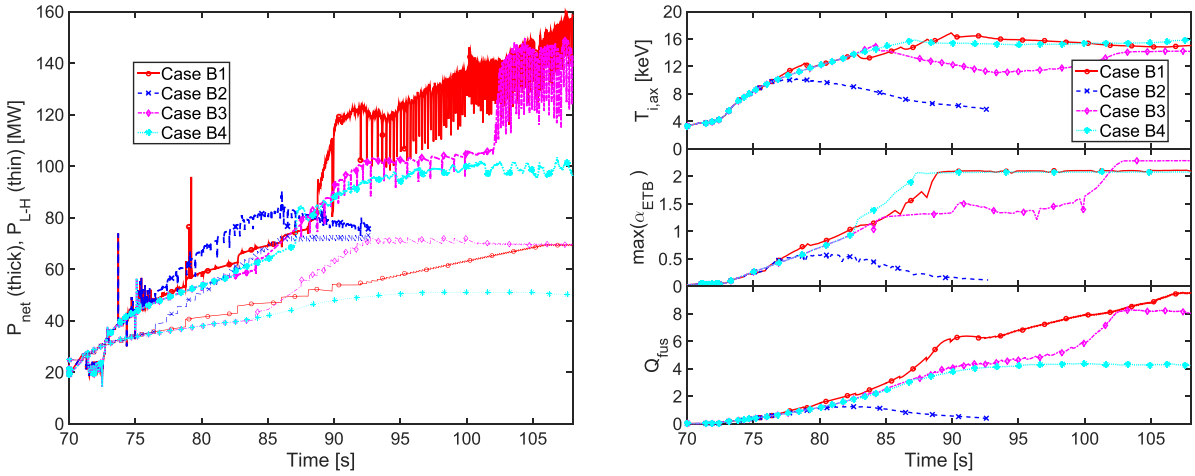

Figure 6. Left: time evolution of net power (thick lines) vs. L-H transition power threshold (thin lines), right: time evolution of the ion temperature on axis (top), the maximum normalised pressure gradient in the ETB (middle) and fusion Q (bottom) from the end of ramp-up at 15 MA, for Cases B1–B4 as described in section 3.2.

the target of 10 MWm^{-2}, the Ne puff rate is strongly increased before stationary ELMy H-mode conditions at high Q_{fus} are reached.

Following considerations in [19], four simulation cases with NB heating applied at $t > \sim$72.5 s and varying strategies for the increase in core density after the L-H transition have been modelled:

B1. Density maintained at a low level for ∼5 s, then slowly ramped up to $n_{e,lin.-avg.} \sim 10^{20}$ m^{-3} by pellets within ∼30 s, injecting standard size pellets for the first 15 s, followed by pellets of reduced size in the later density ramp phase.
B2. Density maintained at a low level for ∼5 s, then quickly ramped up to $n_{e,lin.-avg.} \sim 10^{20}$ m^{-3} by standard size pellets within ∼10 s.
B3. Density maintained at a low level for ∼12 s, then quickly ramped up to $n_{e,lin.-avg.} \sim 10^{20}$ m^{-3} by standard size pellets within ∼10 s.
B4. Density increased by gas fuelling only, no pellet injection.

The plasma evolution for these four cases is shown in figures 5–9.

As the ratio between the net power flux crossing the separatrix P_{net} and the L-H transition threshold P_{L-H} is found to stay close to 1.0 before P_α starts to be significant (see figure 6, left), the density needs to be kept at a low level after the L-H transition until the fusion reaction process sets in, that is until the core plasma ion temperature reaches values of ∼10 keV (see figure 5, right, figure 6, right). As soon as alpha heating becomes significant and P_{net}/P_{L-H} increases significantly above 1.0, the density can be ramped up to its $Q_{fus} \sim 10$ target value by pellets (see figure 5, right, figure 6, right). If the density ramp starts right after the L-H transition or the density is increased too quickly when the plasma is in low density H-mode conditions, P_{net}/P_{L-H} can approach or even drop below the level of 1.0 (see figure 6) and the plasma remains in a degraded type-III ELMy H-mode like regime or eventually returns back to L-mode (see [18, 19]). To ensure a fast increase in alpha heating after the L-H transition, the density needs to

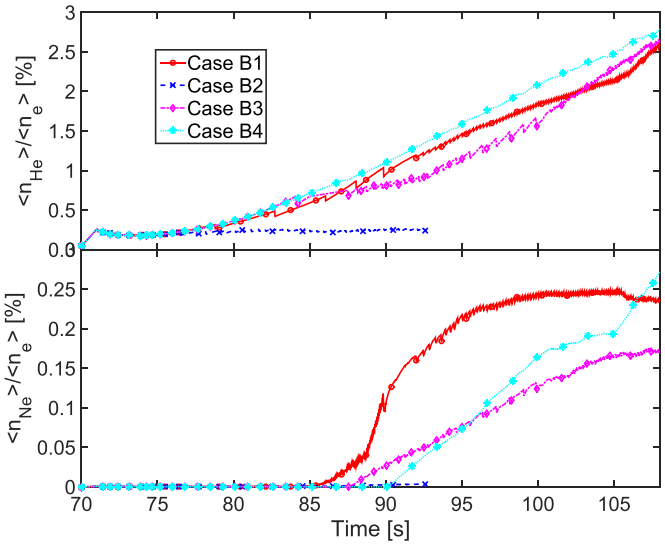

Figure 7. Time evolution of He (top) and Ne (bottom) core concentration from the end of ramp-up at 15 MA, for Cases B1–B4 as described in section 3.2

be ramped such that the ion temperature in the core remains well above a critical level of $T_{\mathrm{i,crit}} \sim 10$ keV for the cross section of the DT reaction to be sizeable [19]. This density ramp must be performed by pellet fuelling; if no pellets are applied, it is not possible to reach $Q_{\mathrm{fus}} \sim 10$ (see results for Case B4), as the core density would remain lower than required to achieve $Q_{\mathrm{fus}} \sim 10$. This core density level is solely determined by the achievable edge density with gas puff only (see [5, 12]).

This requirement for a delayed and gradual ramp in density to access $Q_{\mathrm{fus}} \sim 10$ needs to be reconciled with the need to reduce flux consumption in the H-mode access phase to maximise burn length. This requires that the transition to a stationary burning H-mode regime at $Q_{\mathrm{fus}} \sim 10$ is achieved as quickly as possible. Simulation results indicate that the optimum strategy to achieve this goal is to maintain the density at a low level for ∼5–10 s after the L-H transition and then to apply a ramp in density by pellets to a target Greenwald density fraction of ∼60%–90% within ∼10–20 s, confirming results from more detailed transition scans by means of core + edge transport modelling alone in [19].

The optimization of the access to $Q_{\mathrm{fus}} \sim 10$ also includes core-edge integration aspects that must be addressed to ensure that the solution found provides a fully integrated scenario solution. In this respect, it is important to ensure that good neoclassical impurity screening in the pedestal is maintained in this access phase, which prevents edge impurities (W from the divertor and injected Ne to control divertor radiation) to penetrate into the core plasma. This can be achieved if the ratio between the ion temperature and ion density gradients in the pedestal $\mathrm{d}T_{\mathrm{i,ped}}/\mathrm{d}n_{\mathrm{i,ped}}$ remains sufficiently high [19, 62]. This goal can be achieved by allowing the pedestal temperature to build near to its ELMy H-mode value in the initial low density H-mode phase before the density is increased by pellet fuelling. Since the pedestal evolves very slowly after the L-H transition due to high edge transport because $P_{\mathrm{net}}/P_{\mathrm{L\text{-}H}}$ stays close to 1.0, it takes ∼10 s for the pedestal to build up significant temperature gradients. This determines the time at which pellet fuelling can be applied to ramp the density to its $Q_{\mathrm{fus}} \sim 10$ target value while maintaining good impurity screening. Starting the density ramp by pellet fuelling somewhat earlier (∼5 s) is possible from the point of view of ensuring access to $Q_{\mathrm{fus}} \sim 10$ to maximize burn length but does not ensure good pedestal impurity screening and thus may lead to increased core plasma contamination in this phase.

Similarly, it is important to ensure that also during the access to high Q_{fus} divertor power fluxes remain under the 10 MWm^{-2} limit and the divertor plasma temperature remains below 5 eV to ensure low divertor W sputtering (see figure 9). In this regard, our simulations show that no Ne puff is required for the first few seconds after the L-H transition when the density is maintained at a low level ($<n_{\mathrm{e}}> \sim 0.3$–$0.5\ n_{\mathrm{GW}}$) and the plasma is still in ELM free H-mode phase during which P_{fus} remains low (see figure 5, right, figure 7). However, Ne seeding needs to be applied before the pedestal is fully developed to ensure that the maximum heat flux on the divertor targets remains below 10 MWm^{-2} when the (time-averaged) heat flux crossing the separatrix increases (by ∼20–25 MW) when the ELMy H-mode phase starts (see pre- and post-ELM profiles in figure 9) and the pedestal pressure saturates as a consequence of the triggering of ELMs (modelled by the continuous ELM model); this typically occurs in time scales comparable to the energy confinement time $\tau_{\mathrm{E}} \sim 2.5$ s. The build-up of the Ne density in this time-varying plasma conditions is not a trivial process as the Ne is injected at the divertor while both the power flux into the SOL and the edge density are varying and thus one should avoid over-fuelling that may lead to full detachment and under-fuelling that may lead to excessive power loads and significant W sputtering, and this requires careful tuning of the Ne fuelling rate in our simulations. In practice, this issue will be more complex in ITER since it takes a few hundred milliseconds for Ne gas to arrive in the plasma vessel [63] due to the position of the fuelling valves (away from the plasma to minimize neutron irradiation) and the length of the corresponding pipes (several tens of meters). This time delay is not taken into account in our simulations that assume an instantaneous response of the Ne arriving in the SOL to changes in the requested Ne puff rate; this model is being refined to account for realistic time delays.

Our simulations show that to maintain the maximum heat flux on the divertor targets below 10 MWm^{-2} and to keep the ion temperature in vicinity of the strike points below ∼5 eV to minimise W sputtering, a DT gas puff rate of the order of ~ 1.0–$1.5 \cdot 10^{22}\ \mathrm{s}^{-1}$ needs to be applied in the low H-mode density phase after the L-H transition. Later on, when the density is ramped up by pellets, the DT gas puff rate needs to be increased to $\sim 2.0 \cdot 10^{22}\ \mathrm{s}^{-1}$ to ensure that the divertor can provide the required radiation to maintain divertor heat fluxes under 10 MWm^{-2} as the alpha heating starts to build up (figure 9); at this stage no Ne is required to be injected to achieve this. Finally, as the alpha heating increases with increasing density by pellet fuelling and the pedestal pressure starts to saturate, Ne seeding is required. At this stage the DT gas puff rate is reduced to $\sim 1.0 \cdot 10^{22}\ \mathrm{s}^{-1}$ to avoid

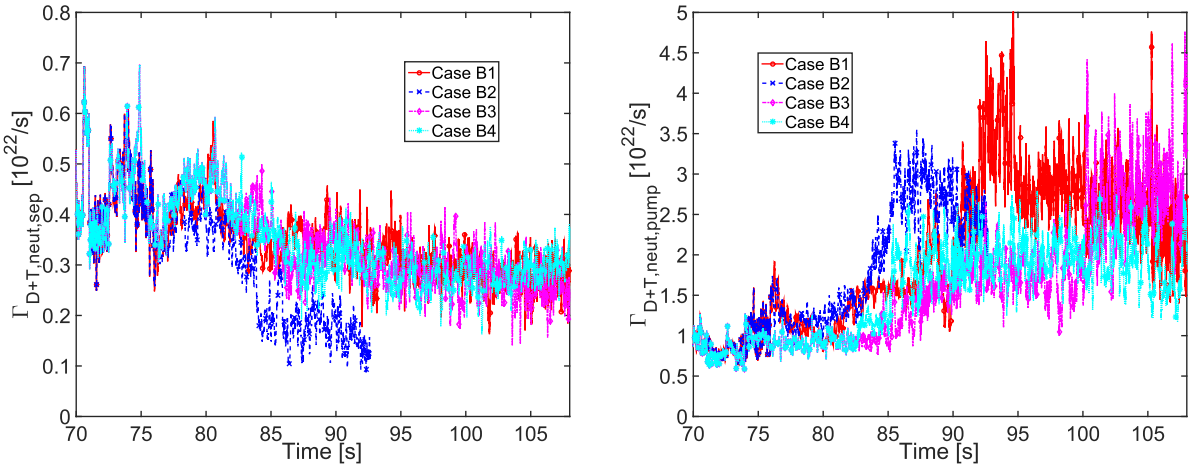

Figure 8. Time evolution of D + T neutral influx at the separatrix (left) and D + T pump rate (right) from the end of ramp-up at 15 MA, for Cases B1–B4 as described in section 3.2.

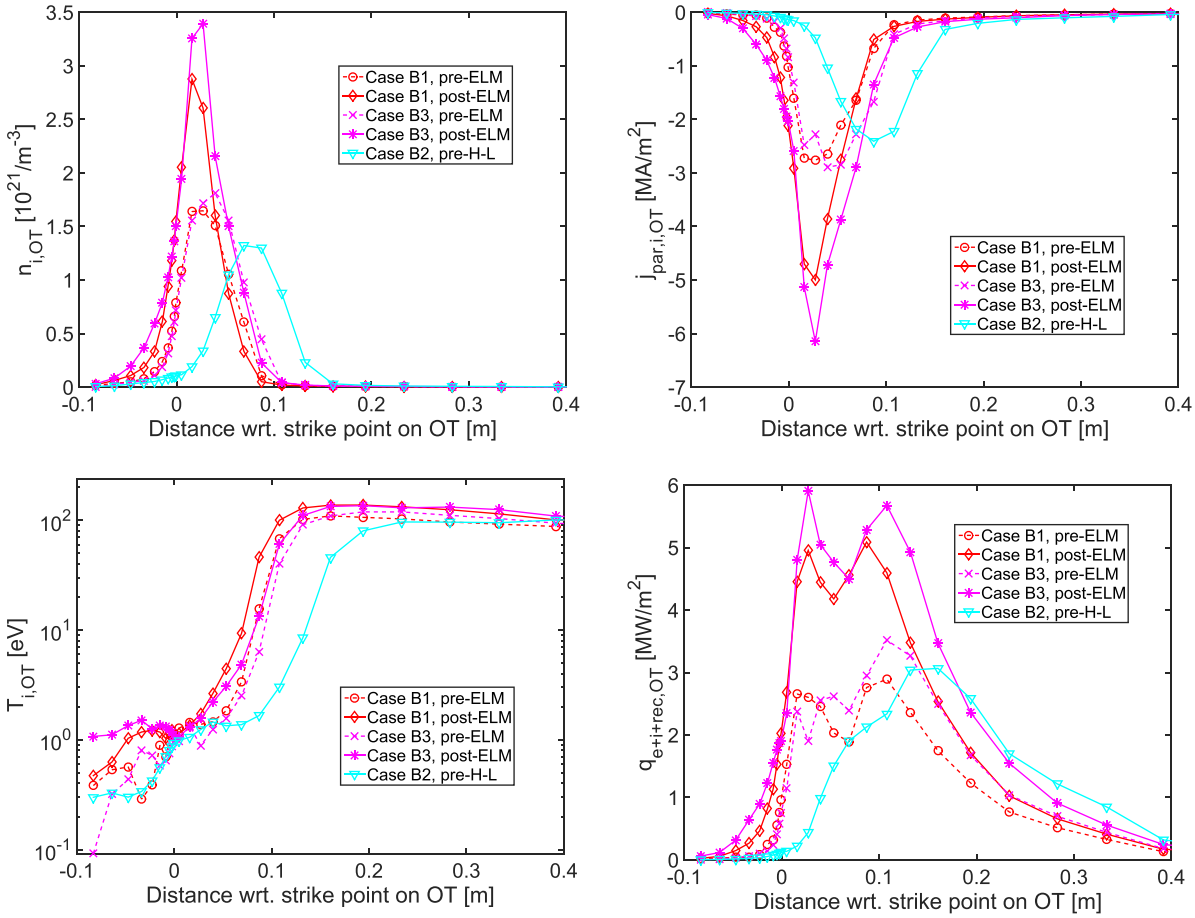

Figure 9. Profiles of ion density, parallel ion flux, ion temperature and power density (from top left to bottom right) at the outer target for Cases B1 (red) and B3 (magenta) before (dashed) and after the onset of ELMs (solid), and for Case B2 before back transition to L-mode (blue) as described in section 3.2.

complete divertor detachment being triggered by the increase in divertor radiation resulting from the injected Ne. With all these adjustments of gas, pellet and Ne fuelling rates, it is possible to design robust scenarios to access $Q_{fus} \sim 10$ with acceptable divertor power fluxes and providing divertor conditions for low W sputtering near the divertor strike zone as shown in figures 5–9 for cases B1 and B3 (although it should be noted that W sputtering might become noticeable in high temperature regions further away from the divertor strike zone where the ion flux may still be non-negligible just after the onset of ELMs for the conditions modelled for cases B1 and B3 as illustrated in figure 9). In stationary burning conditions,

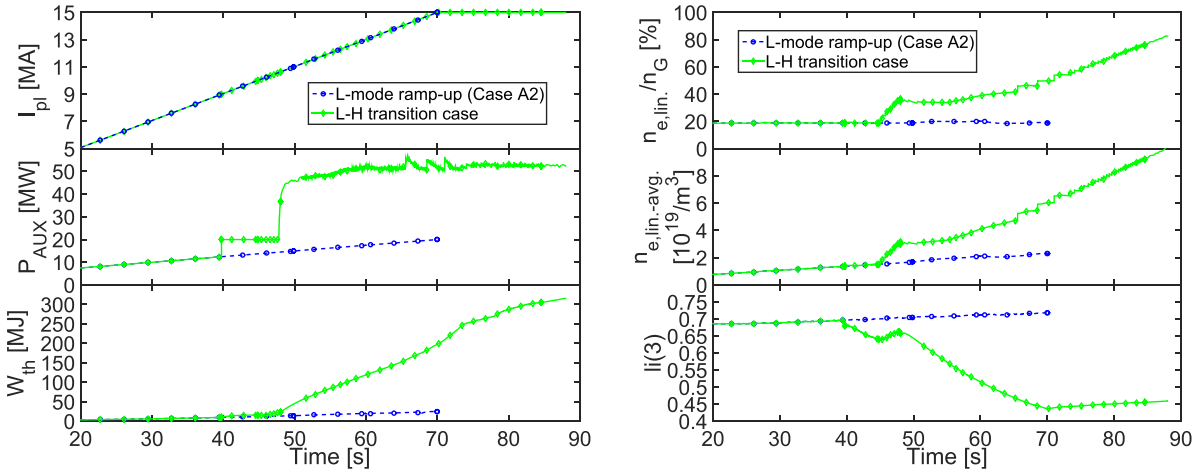

Figure 10. Left: time evolution of plasma current (top), auxiliary power (middle) and thermal core energy content (bottom), right: time evolution of Greenwald density fraction (top), line-averaged electron density (middle) and internal inductance li(3) for an early L-H transition at I_{pl}∼10 MA (green solid), compared to a similar current ramp-up configuration without L-H transition (blue dotted, Case A2 from section 3.1.2).

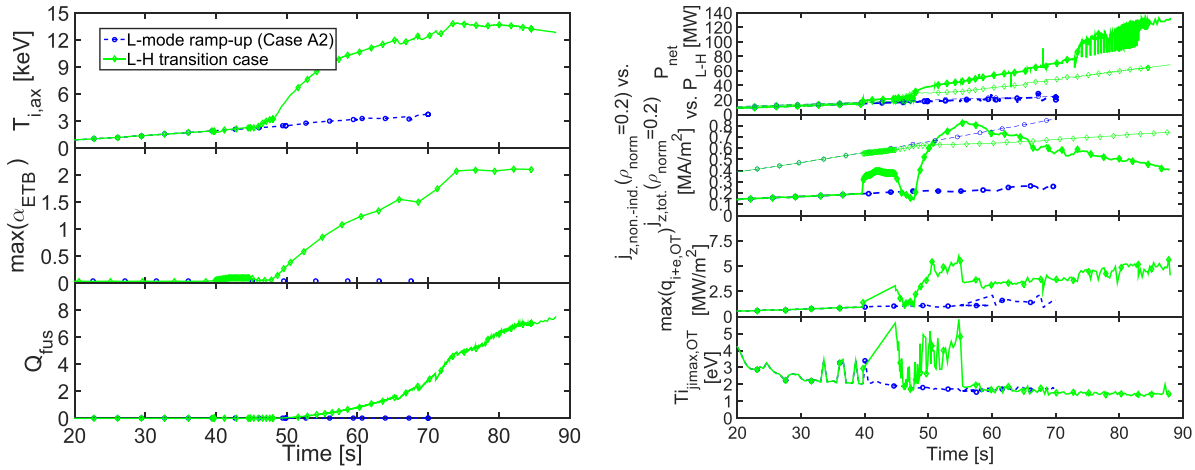

Figure 11. Left: time evolution of the ion temperature on axis (top), the maximum normalised pressure gradient in the ETB (middle) and fusion Q (bottom), right, from top to bottom: time evolution of the net power (thick) vs. the L-H transition power threshold (thin), the non-inductive (thick) vs. total (thin) current density in the plasma centre ($\rho_{norm} = 0.2$), the maximum power density at the outer target and the ion temperature at the outer target location with the maximum absolute value of ion flux density, for an early L-H transition at I_{pl}∼10 MA (green solid), compared to a similar current ramp-up configuration without L-H transition (blue dotted, Case A2 from section 3.1.2).

Ne puff rates to sustain core-edge integrated $Q_{fus} \sim 10$ plasmas in ITER are found to be of the order of $\sim 10^{19}$ s^{-1} in our modelling.

3.3. Access to high Q_{fus} by triggering the L-H transition during the current ramp at ∼10 MA and increasing the plasma density in the follow-up phase to 15 MA

This section is dedicated to the analysis of advantages as well as possible challenges related to current diffusion, core transport and fuelling to be considered if the L-H transition is triggered already during the current ramp-up phase. Strategies for density and divertor control are suggested to access a stationary high Q_{fus} burning regime in case of an early L-H transition at I_{pl}∼10 MA that may be compatible with major operational constraints.

The current ramp-up simulation Case A2 as described in section 3.1.2 has been continued from I_{pl}∼9 MA, including He and bundled Ne impurities. The plasma evolution for the simulation with an early L-H transition is shown in figures 10 and 11 in green. For comparison, simulation results for Case A2 from the current ramp-up scan in section 3.1.2 (current ramp-up with plasma maintained in L-mode) are also shown in blue.

As for the L-H transition cases at the current flat-top of 15 MA that have been described in section 3.2, small (r_p = 2 mm, N_p∼2.1 · 10^{21}) pellets need to be injected in the L-mode ramp-up plasma to achieve a line-average density of $n_{e,lin.-avg.} \sim 3 \cdot 10^{19}$/m^3 that ensures low NB shine-through losses (see figure 10, right). As mentioned above, lower I_{pl} operation in L-mode leads to wide SOL power fall-off lengths both because of edge (q^2 scaling of Bohm/gyro-Bohm transport) and SOL transport (long connection length), which

favours detachment to set in at lower plasma densities. To avoid this happening at the level of plasma density required for NBI injection, the EC power is doubled compared to the reference L-mode ramp-up (case A2) from 10 to 20 MW at I_{pl}∼10 MA before the density is increased by pellet fuelling to $n_{e,lin.-avg.}$∼$3 \cdot 10^{19}$ m^{-3} (see figure 10). At this point I_{pl}∼11 MA and full NB power of 33 MW is applied and the transition to H-mode is triggered (see figure 11, right). In these simulations, NB sources are modelled by ASCOT [42, 43]. ASCOT models properly the beam particle thermalisation time which can delay the transition to H-mode by a few seconds for low initial $P_{net}/P_{L\text{-}H}$ compared to that expected from the NB power waveform (i.e. the NB power takes few seconds in ITER to be absorbed by the thermal plasma before it is conducted to the edge leading to the H-mode transition).

After the start of NB heating, the density is then maintained at an approximately constant level to prevent full divertor detachment and to allow for the increase in pedestal and central ion temperature resulting from the initial H-mode phase. This strategy maintains the net heat flux above the L-H transition power threshold and allows alpha heating to increase in the plasma core (see figure 11). After ∼10 s with respect to the NB switch-on time, the density is gradually ramped by standard ITER size pellets ($r_p = 2.86$ mm) at a frequency of ∼0.3–0.6 Hz for $t < 73$ s and by pellets of reduced size ($r_p = 1.8$ mm) at a frequency of ∼2–10 Hz for $t > 73$ s to the nominal value for $Q_{fus} \sim 10$ in ∼30 s using pellet injection feedback control to access a stationary high confinement H-mode burning plasma regime (see figure 10, right, figure 11, left).

The simulation shows that the transition to high Q_{fus} is more complex to achieve and takes more time when entering H-mode in the current ramp than when this is performed at 15 MA for our modelling assumptions. There are two reasons for this: the first one is the fact that in our modelling the core transport scales unfavourably with q and s/q and the transition to H-mode in the ramp-up phase leads to delayed current penetration and thus lower s/q which decreases core plasma temperatures and fusion power during the ramp-up (see [1, 64]). Due to predictions of reduced particle confinement times in these conditions, an increase in the pellet injection frequency of ∼15%–30% is required in the density ramp phase for the same density ramp configuration in terms of the density ramp rate and selected pellet size as compared to Case B1. The second one is related to the need to increase the plasma density beyond the shine-through limit before the L-H transition in order to apply NB heating and to the dependence of the MHD limit for the H-mode pedestal pressure p_{ped} on plasma current ($p_{ped} \propto I_{pl}$ [37]). As a consequence, the achievable plasma temperature remains lower than 10 keV for the first ∼10 s after the application of the NB. It takes up to 20 s after the NB application for the fusion power to be significant ($Q_{fus} \sim 5$) and the H-mode plasma to reach a robust high confinement regime (see figure 11, left).

On the positive side core-edge integration issues are much simpler in this strategy to access the H-mode than when the H-mode is accessed at 15 MA. This is due to increased transport at higher q and larger connection lengths in the SOL, yielding an increased spread in heat flux along the divertor targets. It is therefore possible to maintain the power flux to the divertor target below 10 MWm^{-2} and to keep the ion temperature in the vicinity of the strike points below ∼5 eV right after the L-H transition with very modest DT gas puffing ($\Gamma_{DT} \sim 0.5 - 1.0 \times 10^{22}$ s^{-1}, see figure 11, right). For later phases when I_{pl} approaches the flat top value and $Q_{fus} \sim 10$, Ne seeding and DT fuelling require similar values to those when the H-mode transition takes place at 15 MA since the conditions of the plasma are similar as well. Section 3.4 illustrates this in more detail.

It is important to note that if the H-mode is accessed in the ramp-up phase, the I_{pl} ramp rate may need to be re-adjusted from the L-H transition onwards, as compared to a pure L-mode ramp-up. This has not been done in our simulations since we aim at comparing the access to high Q_{fus} with H-mode transition in the ramp-up to a pure L-mode ramp-up with access to high Q_{fus} in the flat top. As a consequence, the internal inductance drops to very low values li(3) < ∼0.6 (see figure 10, right), which are not compatible with appropriate plasma shape control [1, 50]. Further optimisation of this scenario to access high Q_{fus} with an L-H transition in the ramp-up is required. To perform this optimisation, a new capability to iterate the JINTRAC code (which uses fixed boundary equilibria) with DINA (which evaluates free boundary equilibria) has been developed within IMAS (Integrated Modelling and Analysis Suite) with initial results presented in [65].

It is also worth noting that the non-inductive current fraction can become significant (∼40%–50%) in the early phase after the L-H transition when the density is kept low, in agreement with previous evaluations [66, 67]. In the central plasma region, the non-inductive current density by the NB can exceed the total current density triggering the appearance of a negative voltage in the core; this can potentially give rise to the formation of a current hole (see figure 11, right) revealing the need for further optimisation of the scenario (i.e. delaying the L-H transition to $I_{pl} > 10$ MA or with a different heating mix with lower NB heating and current drive contribution).

3.4. Full simulations of access to high Q_{fus} stationary burning plasmas at 15 MA

Figure 12 summarises a subset of the key simulations of the plasma evolution from early current ramp up to high Q_{fus} performed in our studies. Five strategies were defined that are:

a. Red dashed: L-H transition at $I_{pl} = 15$ MA, slow density ramp by pellets, successful transition to high Q_{fus} (combination of Cases A1 + B1).
b. Blue dotted: L-H transition at $I_{pl} = 15$ MA, fast density ramp by pellets, unsuccessful transition to high Q_{fus} (Cases A1 + B2).
c. Magenta solid: L-H transition at $I_{pl} = 15$ MA, delayed fast density ramp by pellets, successful transition to high Q_{fus} (Cases A1 + B3).
d. Green dash-dotted: L-H transition at I_{pl}∼10 MA, delayed slow density ramp by pellets, successful transition to

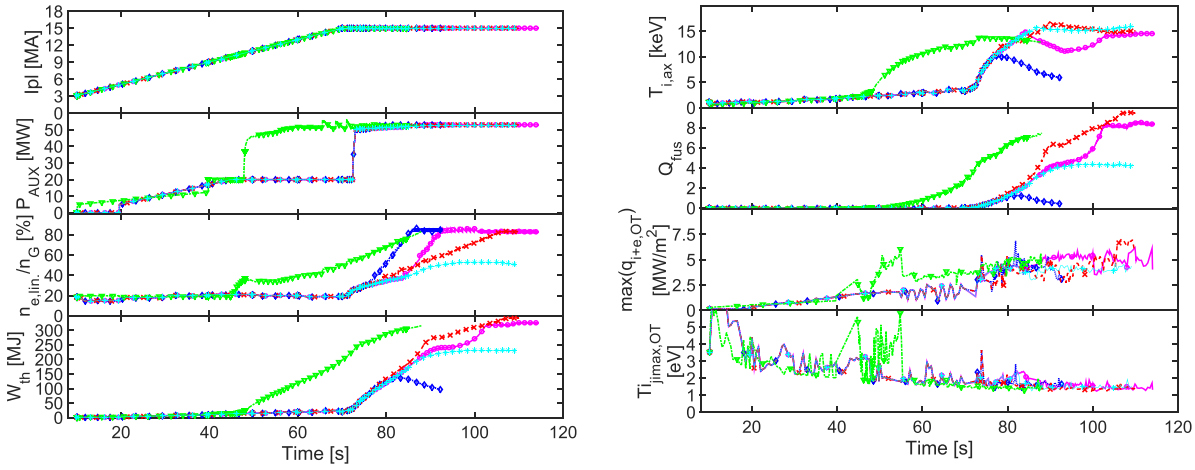

Figure 12. Left, from top to bottom: time evolution of plasma current, auxiliary power, Greenwald density fraction, thermal energy content, right, from top to bottom: time evolution of ion temperature on axis, fusion Q, the maximum power density at the outer target (considering power transferred by electrons, ions and due to recombination) and ion temperature at the outer target location with the maximum absolute value of ion flux density, from early current ramp-up at 3 MA to good quality H-mode for the following cases: red crosses: Case A1 from section 3.1.2 and Case B1 from section 3.2, blue diamonds: Case A1 from section 3.1.2 and Case B2 from section 3.2, magenta circles: Case A1 from section 3.1.2 and Case B3 from section 3.2, green triangles: Case A2 from section 3.1.2 until $I_{pl}\sim$9 MA, followed by the early L-H transition case from section 3.3, cyan stars: Case A1 from section 3.1.2 and Case B4 from section 3.2.

high Q_{fus} (Cases A2 + early L-H transition case from section 3.3).

e. Cyan thin solid: L-H transition at $I_{pl} = 15$ MA, no density ramp by pellets, successful transition to moderate Q_{fus} (Cases A1 + B4).

The results of figure 12 demonstrate that it is possible to achieve and maintain the two main criteria for core-edge integration in these scenarios for $Q_{fus}\sim 10$ operation throughout all the phases considered, namely acceptable divertor power fluxes and low W sputtering ($\max(q_{target}) < 10$ MWm^{-2}, $T_{i,jmax,OT} < \sim$5 eV). JINTRAC simulation results show that viable plasma scenarios to achieve the ITER target of $Q_{fus}\sim 10$ can be designed with the baseline heating and current drive system, DT fuelling and impurity injection systems with the plasma evolution successfully controlled to respect all major operational limits.

4. Stationary high Q_{fus} simulations and exit phase from high Q_{fus} and current ramp-down

4.1. Simulation of stationary H-mode at $Q_{fus}\sim$10 with discrete pellet fuelling

Results from an integrated core-edge-SOL simulation for quasi-stationary high Q_{fus} burning conditions considering discrete pellet fuelling, the transport of He ash and feedback controlled Ne seeding are presented and analysed hereafter.

The JINTRAC simulations for gas and pellet fuelled high Q_{fus} H-mode plasmas at $I_{pl} = 15$ MA and $B_0 = 5.3$ T at $P_{AUX} = 53$ MW (33 MW NB + 20 MW EC power) with W target that have been presented in section 3.2 have been repeated at a fixed D + T gas puff rate of $\Gamma_{DT,neut} = 10^{22}$ s^{-1} with Ne seeding. He and (bundled) Ne impurity transport are also taken into account. Ne seeding is adjusted by feedback control (assuming an ideal and instantaneous feedback control with a zero feedforward control puff rate) in order to maintain a Ne radiation level in the SOL and divertor of $\sim$30 MW, which gives an averaged Ne concentration in the SOL and divertor of $\sim$0.5%. Pellets with a 1:1 D-T mixture and a size of $r_p\sim$2.8 mm ($N_p\sim 6.1\cdot 10^{21}$) are injected at a speed of $v_p = 300$ m s^{-1} from the upper of the two available injection lines at the lower High Field Side [68]. The pellet injection frequency is adjusted by a feedback control scheme in order to maintain a line-averaged electron density of $\sim$1.0–$1.05\cdot 10^{20}$/m^3 ($\sim$85% of n_{GW}) which requires a typical injection frequency of $\sim$2.0–2.5 Hz, which is in line with previous core transport fuelling studies [29]. He is produced by fusion reactions in the core and the simulation is continued for almost 100 s until stationary conditions are approached for the He density in the core and edge regions. The results of the simulations are shown in the figures 13–16:

Our simulations show that the maximum power density on the inner and outer targets, $\max(q_{IT})$ and $\max(q_{OT})$, can be maintained below 10 MWm^{-2} with the applied D + T and Ne puff rates and the divertor temperature can also be maintained below $\sim$5 eV in the region of maximum divertor ion flux (see figure 16). It should be noted that these simulations do not include cross-field drifts in the SOL and this can affect the level of in-out power asymmetries. The inclusion of these drifts is technically challenging due to numerical stability issues; we expect that when these are overcome and integrated simulations with SOL drifts are possible, the Ne seeding and fuelling rates will have to be re-optimised to maintain power fluxes under 10 MWm^{-2} at both divertor targets.

Analysis of the SOL power fall-off length near the separatrix for these simulations provides $\lambda_q\sim$1–2 mm; these are in agreement for Scan 1 in table 1 in [5] and not far from those estimated from empirical scalings for ITER 15 MA $Q_{fus}\sim 10$

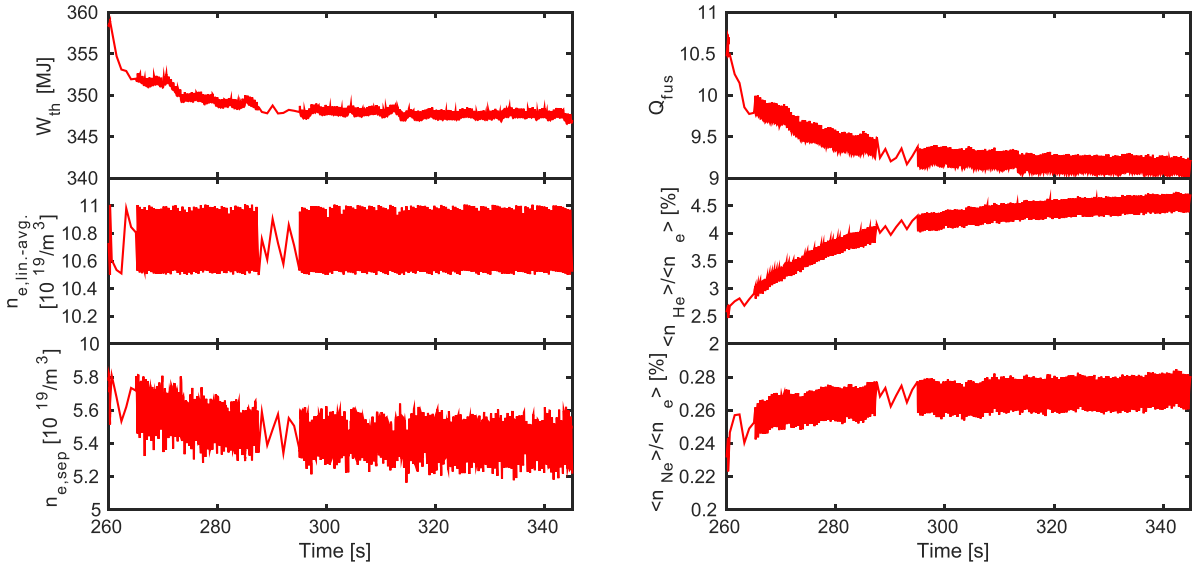

Figure 13. Left: time evolution of thermal energy content, line-averaged electron density and electron density at the separatrix, right: time evolution of fusion Q, the He core concentration and the Ne core concentration (from top to bottom) for the pellet and gas fuelled high Q_{fus} D + T H-mode plasma described in section 4.1.

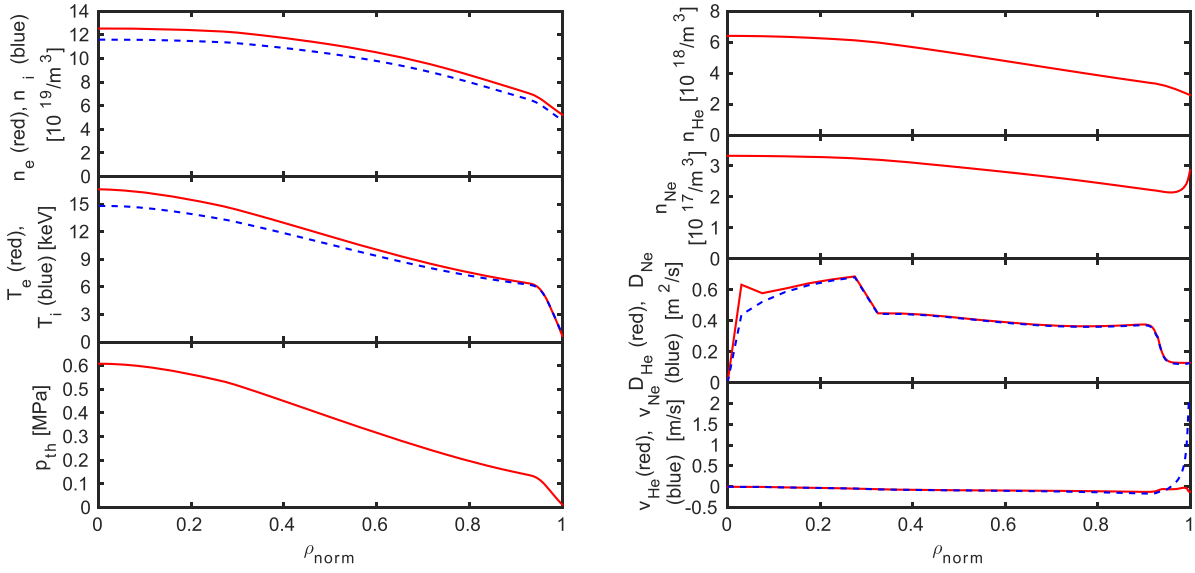

Figure 14. Left: plasma profiles of electron (red solid) and ion (blue dashed) density (top), temperature (middle) and thermal pressure (bottom), right: plasma profiles of He density, Ne density, He (red solid) and Ne (blue dashed) diffusivity and convection velocity (from top to bottom), at t∼318.8 s (close to stationary conditions) for the pellet and gas fuelled high Q_{fus} D + T H-mode plasma described in section 4.1.

H-mode plasmas [69]. These values are significantly smaller than those estimated for the same plasma conditions by recent gyrokinetic modelling, which give $\lambda_{\mathrm{q}} = \sim$5–6 mm [70] due to enhanced heat transport driven by non-linear edge turbulence effects not considered in our simulations that can be thus considered conservative in this respect. It is important to note that the divertor power flux profiles in semi-detached conditions do not often show a simple exponential decay. This is the result of power dissipation in the divertor, which can be dominant near the separatrix, as well as of our assumptions on the radial profile of edge transport coefficients that increase away from the separatrix in these H-mode plasmas.

The injection of pellets can also significantly modify the divertor power flux profiles, particularly immediately after the injection of a pellet. This is seen to some degree in our simulations (see figure 16), where some divertor power flux profiles during the pellet cycle are shown, and is discussed in more detail in [22, 71], together with the specific challenges for the control of divertor power fluxes in high radiative divertor conditions.

The He density at the separatrix saturates at $n_{\mathrm{He,sep}}\sim 2.5\cdot 10^{18}/\mathrm{m}^3$, while the He density on axis approaches $n_{\mathrm{He,ax}}\sim 6\cdot 10^{18}/\mathrm{m}^3$, corresponding to a core He peaking factor of $n_{\mathrm{He,ax.}}/\mathrm{n}_{\mathrm{He,sep}}\sim$2.4 and core He concentration of ∼4.5%

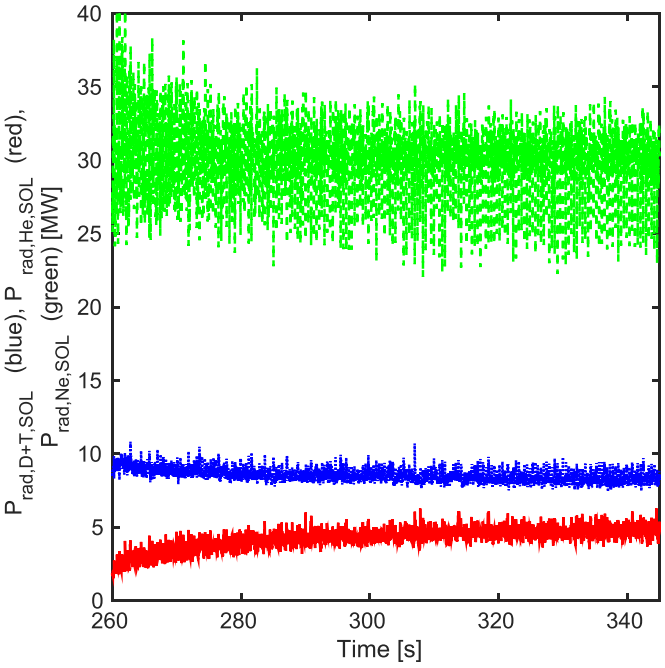

Figure 15. Time evolution of D + T (blue dotted), He (red solid) and Ne (green dashed) induced radiation in the SOL and divertor for the pellet and gas fuelled high $Q_{\rm fus}$ D + T H-mode plasma described in section 4.1.

(see figure 13, right, figure 14, right). This peaking factor is considerably larger than that obtained in core-only simulations with the GLF-23 transport model [28] with comparable $n_{\rm He,ax}$ as described in [22]. This is due to different assumptions for the He core diffusivity in our simulations and those with GLF-23. In the present work, $D_{\rm He}$ is taken to be identical to the diffusivity for main ions with the BgB model retuned to GLF-23 [29] and thus much lower than $D_{\rm He}$ as predicted directly by GLF-23 [22]. Thus the He transport assumptions made in this work are more conservative regarding He accumulation than assuming the GLF-23 model and despite this we show that $Q_{\rm fus} \sim 10$. By the end of our simulations stationary conditions are achieved for the He content (see figure 13, right) and the time-averaged He pump rate becomes identical to the He source rate due to fusion reactions in the core, $S_{\rm D+T\rightarrow He} \sim 1.75 \cdot 10^{20}$ s^{-1}. As a consequence of the plasma dilution by He, a slight degradation in fusion performance from $P_{\rm fus} \sim 550$ MW to $P_{\rm fus} \sim 490$ MW can be observed, as the He concentration increases from ∼2% to ∼4.5% (see figure 13, right). Despite this He concentration and the use of Ne seeding for edge power control, $Z_{\rm eff}$ remains low (∼1.35) in stationary conditions. This is due to the effective neoclassical temperature screening in the pedestal which provides a low level of $n_{\rm Ne,core} \sim 2.5$–$3.0 \cdot 10^{17}$ m^{-3} ($\langle n_{\rm Ne}\rangle/\langle n_{\rm e}\rangle = \sim 0.25\%$) despite the large SOL + divertor radiation from Ne (see figure 13, right, figure 15). Without the temperature screening effect, the core Ne density would be increased by 30%–40% for the same value of $n_{\rm Ne,sep}$. This moderate $\langle n_{\rm Ne}\rangle$ leads to a low total core radiation in stationary conditions of $P_{\rm rad,core} \sim 25$ MW (consisting of ∼8 MW of Ne radiation, ∼14 MW of bremsstrahlung and ∼3 MW of synchrotron radiation). Other important core parameters in quasi-stationary conditions are: $Q_{\rm fus} \sim 9.0$–9.5, $H_{98,\rm y} \sim 0.95$, $\beta_{\rm N} \sim 2.05$, $P_{\rm sep} \sim 135$ MW.

4.2. Simulations of the exit phase from high Q_{fus} burning plasma conditions and of the current ramp-down

In this and the following two sub-sections, simulations for the exit phase from stationary burning conditions including the ramp-down in current from $I_{\rm pl} = 15$ MA to 3 MA are described, comparing beneficial and challenging properties for cases of an H-L transition occurring at high ($I_{\rm pl} = 15$ MA) vs. low ($I_{\rm pl} = 10$ MA) current. The compatibility with operational constraints is assessed and possibilities for the optimisation of the current ramp-down conditions are discussed. Requirements for the control of the Ne content in the plasma are described and possible remedies for the avoidance of divertor detachment after the H-L transition due to remnant Ne are suggested.

Continuing from the stationary flat-top phase at $Q_{\rm fus} \sim 9$–10 in the previous section, the exit from burning conditions and the following current ramp-down phase have been simulated down to $I_{\rm pl} \sim 3$ MA during which the plasma can be expected to remain in diverted configuration.

To define the most demanding cases for the control of divertor conditions in this phase, we assume that pellet fuelling is switched off for the high $Q_{\rm fus}$ exit and current ramp-down phases. In addition, the auxiliary heating is also switched off instantaneously at a specified current level, to eventually trigger the H-L transition. After the auxiliary heating switch off the plasma quickly transitions from ELMy H-mode into ELM free H-mode, then to a degraded type-III ELMy H-mode and finally returns back to L-mode. When performing the first simulations with these assumptions, it was found that, following the heating switch-off phase, the divertor could become completely detached because of the high separatrix density, divertor radiation and decreased net power flow. This led to the crash of the simulations and would correspond to the formation of a MARFE in experiments. To avoid full divertor detachment, ECRH is thus applied again in the early L-mode phase at $P_{\rm EC} = 10$–20 MW.

D + T and Ne puff rates are adjusted in order to maintain the divertor peak heat load below 10 MWm^{-2}, to keep the divertor plasma temperature below ∼5 eV near the separatrix while avoiding full divertor detachment. The nominal D + T gas puff rate is typically maintained at a level of $\Gamma_{\rm DT,neut} \sim 10^{22}$ s^{-1} in the initial exit phase from high $Q_{\rm fus}$ and then quickly reduced to a very low level before the H-L transition. The Ne puff rate is feedback controlled while the plasma remains in H-mode to maintain a prescribed target level for Ne radiation in the SOL and divertor, and is gradually reduced to zero before the plasma returns back to L-mode. To effectively control the Ne radiation and the divertor power flux, the adjustment of the Ne content is achieved by adjusting its recycling coefficient in these simulations. This may not necessarily correspond to a realistic removal of Ne from the edge by the ITER pumping system but is used to effectively develop a whole core-edge integrated scenario for the high $Q_{\rm fus}$ exit and current ramp-down phase. These results are then used to perform

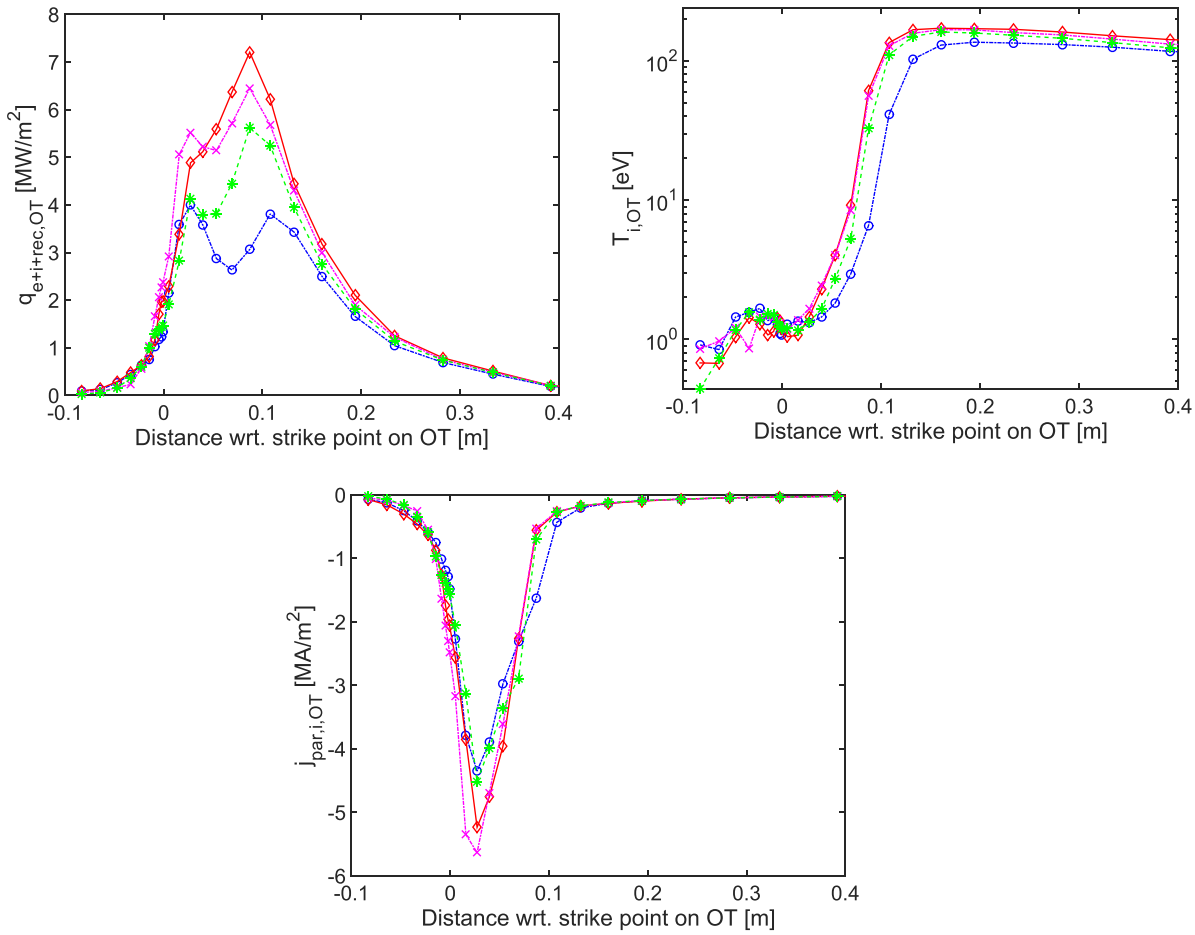

Figure 16. Power flux density (top left, including power from electrons, ions and recombination), ion temperature (top right) and ion flux density (bottom) at the outer target at various time instants during a pellet injection cycle, i.e. 1 ms, 94 ms, 235 ms and 368 ms after the injection of a pellet, for the pellet and gas fuelled high Q_{fus} D + T H-mode plasma described in section 4.1

more detailed studies in which the Ne particle balance is modelled realistically (i.e. Ne gas injection and pumping by the ITER cryo-pump) that are described in section 4.4.

We have modelled two cases for the high Q_{fus} and current ramp-down phase with different times for the H-L transition:

C1. Early H-L transition at current flat-top $I_{pl}\sim$15 MA: auxiliary heating is completely switched off at $I_{pl}\sim$15 MA while the plasma remains in H-mode. Zero edge loop voltage is prescribed for the entire current ramp-down phase.
C2. Late H-L transition at $I_{pl}\sim$10 MA: auxiliary heating maintained in the initial current ramp-down phase and completely switched off at $I_{pl}\sim$10 MA while the plasma remains in H-mode. The edge loop voltage is reduced from 0 V down to −0.1 V in the late H-mode phase to speed up the reduction in plasma current.

The plasma evolution for the high Q_{fus} exit and current ramp-down Cases C1 and C2 is shown in figures 17–23 (early H-L transition at $I_{pl}\sim$15 MA: blue, late H-L transition at $I_{pl}\sim$10 MA: red).

Simulation results shown in figures 17–22 show that exit from high $Q_{fus}\sim 10$ burning plasma conditions with a flat-top current of $I_{pl} = 15$ MA and current ramp-down to L-mode at $I_{pl} = 3$ MA can be achieved by the use of the capabilities of the heating and current drive and fuelling and impurity seeding systems while maintaining acceptable divertor power fluxes and plasma conditions (see figure 17, right, figures 21 and 22) leading to low W sputtering and maintaining core impurity contamination at a moderate level (see figure 19, right) and with it a moderate level of core plasma radiation (see figure 20, right). An important finding of our studies is that the plasma density can be controlled well below n_{GW} by the switch off of pellet fuelling and the pumping provided by the ITER cryo-pumps even for Case C1 which has a higher $|dI_{pl}/dt|$ (see figure 17, left). Similar to the ramp-up, studies with the JINTRAC-DINA-IMAS suite have shown that the above core-edge integrated scenarios respect PF coil current, voltage and magnetic field limits [65].

As shown in figure 19, left, the plasma internal inductance increases significantly towards the end of ramp-down. To ensure proper vertical stability control in this phase, the plasma will be de-elongated in ITER scenarios [20], but this change of plasma shape could not yet be included with the modelling capabilities available at the time when the simulations were carried out. To mitigate that increase, the continued application of P_{AUX} until late ramp-down and a gradual reduction in plasma elongation could be considered.

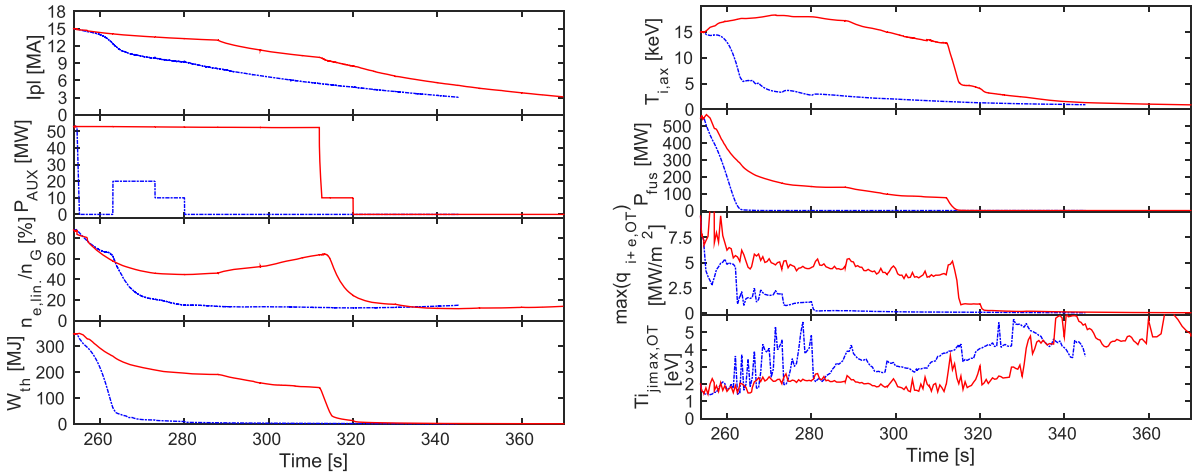

Figure 17. Left: time evolution of plasma current, auxiliary power, Greenwald density fraction, thermal energy content, right: time evolution of ion temperature on axis, fusion power, the maximum power density at the outer target (considering power transferred by electrons, ions and due to recombination) and ion temperature at the outer target location with the maximum absolute value of ion flux (from top to bottom) during the high $Q_{\rm fus}$ exit and current ramp-down for $I_{\rm pl} = 15 \rightarrow 3$ MA for an H-L transition at $I_{\rm pl}\sim$15 MA (blue dash-dotted) and $I_{\rm pl}\sim$10 MA (red solid).

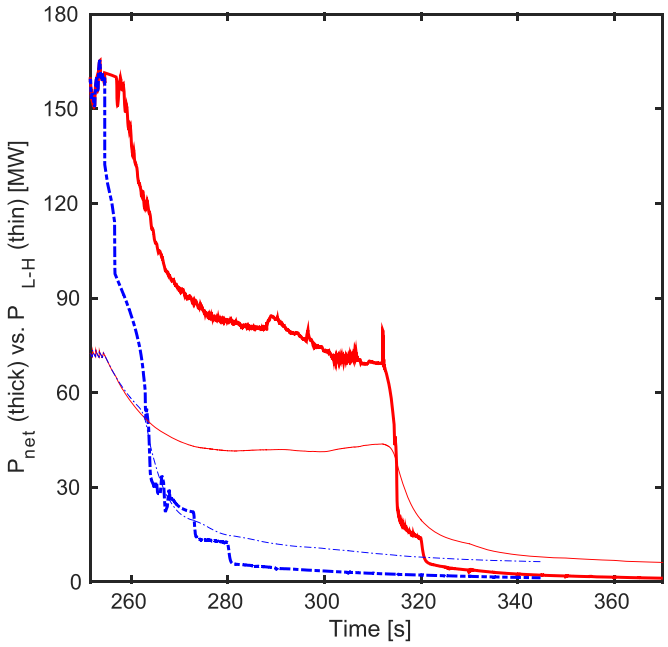

Figure 18. Time evolution of net power (thick lines) vs. L-H transition power threshold (thin lines), during the high $Q_{\rm fus}$ exit and current ramp-down for $I_{\rm pl} = 15 \rightarrow 3$ MA for an H-L transition at $I_{\rm pl}\sim$15 MA (blue dash-dotted) and $I_{\rm pl}\sim$10 MA (red solid).

To facilitate the control of divertor conditions, a late H-L transition at lower plasma current appears to be favourable, because the edge parameters and net power flux evolve in long timescales, and it is easier to adapt Ne radiation. The H-L transition itself takes place in a shorter timescale than for 15 MA (see figure 17, left, figure 18), but the power fluxes involved in this transition are much lower due to the lower $\mathrm{d}W_{\rm th}/\mathrm{d}t$ at this stage and the lower P_α compared to 15 MA (see figure 18, figure 19, left). At the time of the H-L transition at $I_{\rm pl}\sim$10 MA the divertor power flux is lower than 5 MWm^{-2} (see figure 17, right, figure 21, left) and Ne seeding can be safely stopped and Ne be pumped out of the system (see figure 17, right, figure 19, right, figure 20, left).

4.3. Current ramp-down in H-mode at zero loop voltage

The case C2 from section 4.2 with a late transition from H-mode to L-mode at $I_{\rm pl}\sim$10 MA has been rerun with a fixed loop voltage at the boundary of 0 V (referenced as Case C2b). In this case, the temperature remains high ($T_{\rm e,ax}\sim$15–20 keV) while the $P_{\rm AUX}$ remains at 53 MW and the plasma stays in H-mode, while density rapidly falls to $\sim 0.5 \cdot n_{\rm GW}$ after pellet fuelling stops at the beginning of the $I_{\rm pl}$ ramp-down (see figure 23, left). In these conditions, resistive flux losses are very small ($\sim$0.03 Wb s^{-1}, similar to the flat-top phase) and the inductive flux and $I_{\rm pl}$ fall very slowly thus significantly extending the H-mode phase while remaining within the operational limits of the central solenoid, as already identified in [1].

The plasma evolution for the simulation for the case C2b is shown in figure 23 in magenta together with C2 from the previous section in red, for comparison.

Case C2b confirms that the neutron yield can be significantly enhanced by the extension of the H-mode duration by up to a few hundred of seconds into the current ramp-down phase by applying zero boundary loop voltage if the auxiliary heating is maintained but pellet fuelling is switched off at the beginning of current ramp-down. This can be achieved with acceptable divertor conditions (power flux and divertor temperature, see figure 23, right) by decreasing the Ne seeding level gradually. In this case, it cannot be switched off completely since $P_{\rm AUX} = 53$ MW and $I_{\rm pl} \geq \sim$12–13 MA for the 150 s modelled (see figure 23, left). As already demonstrated for Case C2, the control of the Ne concentration may be facilitated for increased H-mode duration, as the available time scales for Ne exhaust from the core are extended in these conditions.

As indicated in the baseline optimisation studies in [1, 72], optimisation of the current ramp-down in H-mode by maintaining $P_{\rm AUX}$ can increase the total neutron fluence of the

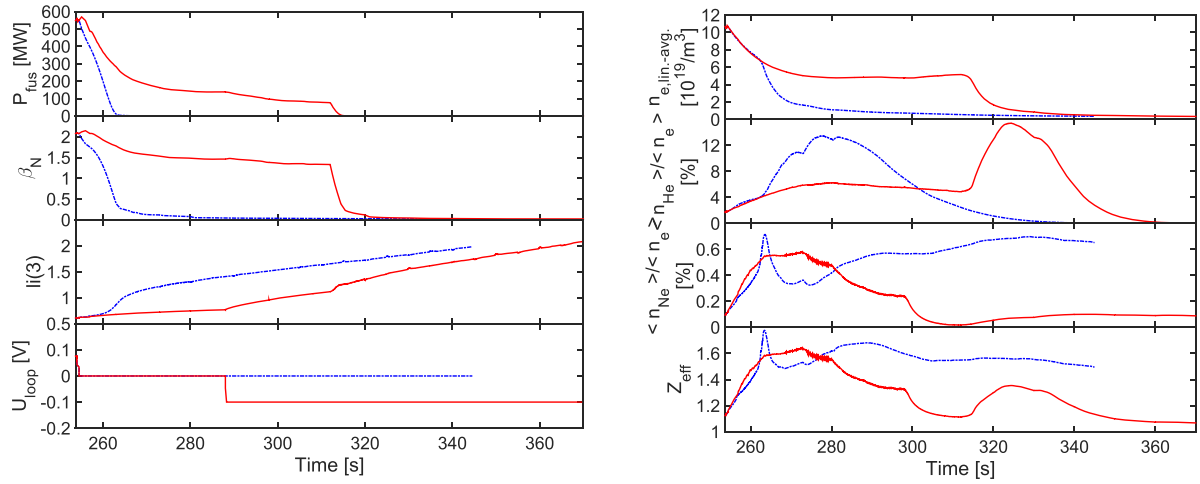

Figure 19. Left: time evolution of fusion power P_{fus}, normalised beta, internal inductance li(3) and loop voltage, right: time evolution of line-averaged electron density, He core concentration, Ne core concentration and Z_{eff} (from top to bottom), during the high Q_{fus} exit and current ramp-down for $I_{\mathrm{pl}} = 15 \rightarrow 3$ MA for an H-L transition at $I_{\mathrm{pl}}\sim$15 MA (blue dash-dotted) and $I_{\mathrm{pl}}\sim$10 MA (red solid).

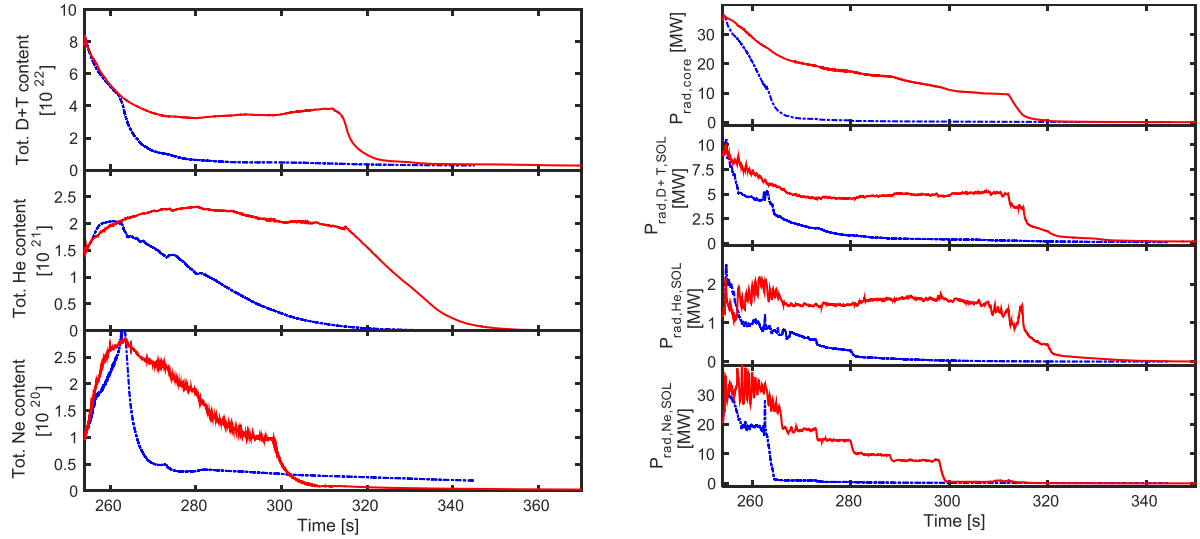

Figure 20. Left: time evolution of total D + T (top), He (middle) and Ne (bottom) ion content in the core, SOL and private region, right: time evolution of core radiation, D + T induced, He induced and Ne induced radiation in the SOL and divertor plasma (from top to bottom), during the high Q_{fus} exit and current ramp-down for $I_{\mathrm{pl}} = 15 \rightarrow 3$ MA $I_{\mathrm{pl}} = 15 \rightarrow 3$ MA for an H-L transition at $I_{\mathrm{pl}}\sim$15 MA (blue dash-dotted) and $I_{\mathrm{pl}}\sim$10 MA (red solid).

$Q_{\mathrm{fus}} \sim 10$ scenario by 50% without additional cycling of the central solenoid.

4.4. Refined simulations of the exit phase from high Q_{fus} burning plasma conditions and of the current ramp-down

The simulations of the transition from stationary high Q_{fus} H-mode to L-mode at $I_{\mathrm{pl}}\sim$15 MA and $I_{\mathrm{pl}}\sim$10 MA that were presented in section 4.2 (Cases C1–2) have been repeated with improved accuracy to refine the requirements for the control of the divertor power fluxes and divertor plasma temperature by D + T puff and Ne seeding with a realistic description of Ne pumping instead of the numeric feedback system with instantaneous response in section 4.2. These new simulations, referred to as Cases D1/1b and D2 for the early and late H-L transition, respectively, have been carried out with increased precision in the calculation of SOL transport (application of adaptive partial coupling with a reduced maximum allowed proportion of the non-coupling and full coupling time intervals $\Delta t_1/\Delta t_2 = 10$), and ensuring correction fluxes for main ions and impurities in the SOL remain $\leqslant\sim$1% with respect to reference fluxes thus avoiding artificial particle sources and sinks being introduced numerically. This is important to accurately model the transient evolution of the SOL plasma on shorter time scales during the H-L transition phase, while the error due to partial coupling with normal accuracy used for Cases C1–2 is insignificant for the slow transients in all other phases during current ramp-down. In addition to this improved accuracy of the partial coupling scheme, the DT and Ne fuelling rates are provided by purely feedforward waveforms for cases D1–2, and this allows precise particle balance for Ne in these simulations, i.e. the evolution of the Ne density in the plasma

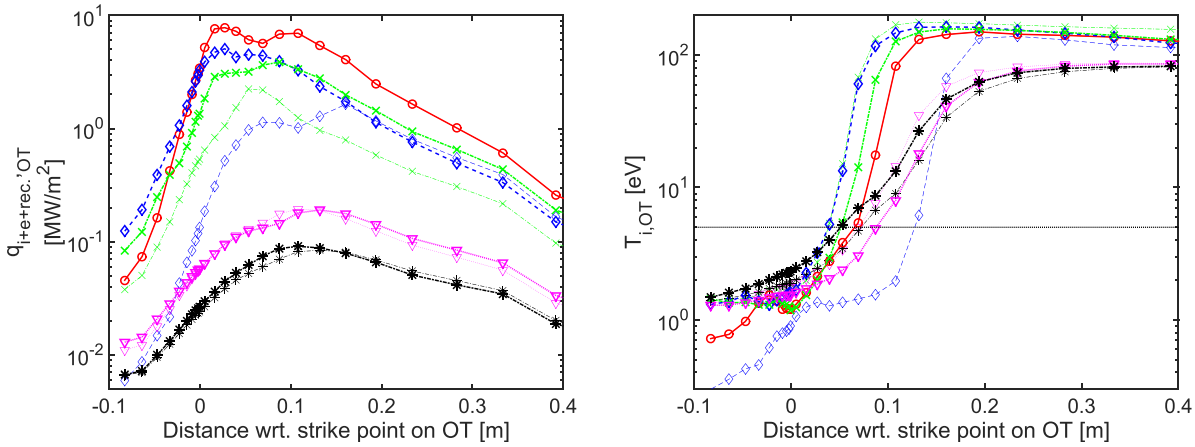

Figure 21. Profiles of power flux density (left) and ion temperature (right) at the outer target (including power from electrons, ions and recombination) at $I_{pl} = 15$ MA (red circles), 12.5 MA (blue diamonds), 10 MA (green crosses), 7.5 MA (magenta triangles) and 5 MA (black stars) during the current ramp-down for an H-L transition at $I_{pl}\sim$15 MA (thin lines) and $I_{pl}\sim$10 MA (thick lines).

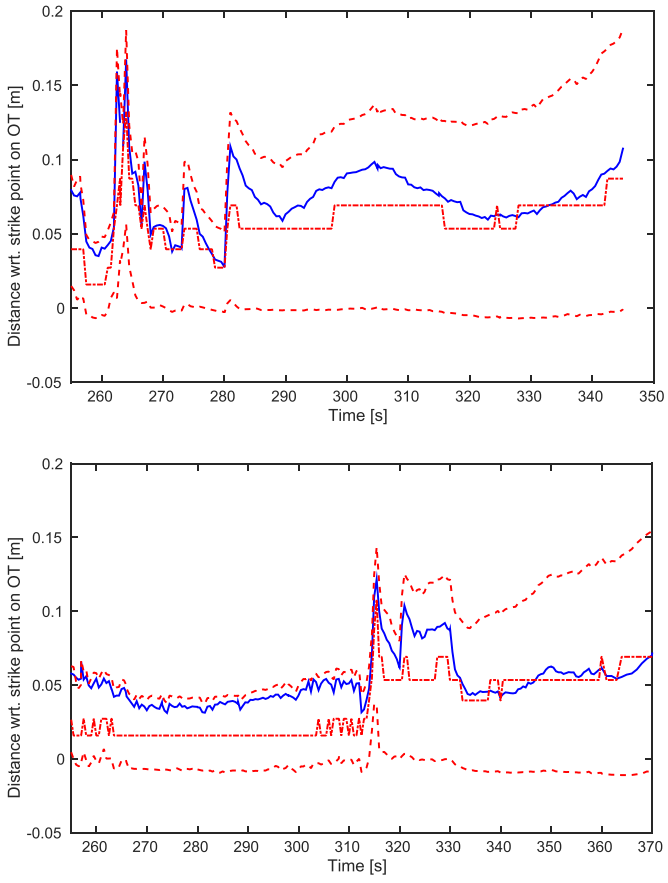

Figure 22. Time evolution of the locations on the outer divertor target where $T_i\sim$5 eV (blue solid), where the maximum ion flux density is reached (red dash-dotted) and where half of the maximum ion flux density is obtained (red dashed) during the current ramp-down for the case of an H-L transition at $I_{pl}\sim$15 MA (Case C1, top) and at $I_{pl}\sim$10 MA (Case C2, bottom).

is the sole result of Ne seeding, transport and exhaust by the ITER cryo-pumps; there is no artificial source or sink of Ne introduced by the numerical scheme in these simulations. The design of the feedforward waveforms for D + T and Ne fuelling is done iteratively by trial and error to maintain divertor power fluxes under 10 MWm^{-2} and the divertor plasma temperature under ∼5 eV near the strike points. The auxiliary heating is completely switched off at the start of the H-L transition phase for Case D1 while a low level of $P_{EC} = 10$ MW is maintained for Cases D1b and D2 (see figure 24, left).

The plasma evolution for the improved calculations of the H-L transition is shown in figures 24–28 (Case D1: blue dash-dotted, Case D2: red solid, Case D1b: cyan dashed).

The simulation results in figures 24 and 25 show that the duration of the transition from good quality H-mode to L-mode is long enough in order to ensure appropriate plasma shape and position control during the transition due to the decreasing plasma energy, as described in [1, 17]. The H-mode energy collapse duration is longer for the transition at high current ($I_{pl}\sim$15 MA: ∼8–10 s, $I_{pl}\sim$10 MA: ∼3 s, see figure 25, left) because the thermal energy content is considerably higher at the start of the H-L transition (see figure 24, left), and because of the alpha heating remaining significant during the transition itself (see figure 24, right).

Figures 24, right, 27 and 28 show that the maximum heat flux on the divertor targets can be kept below 10 MWm^{-2} and the ion temperature in the vicinity of the strike points can be maintained below ∼5 eV by careful adjustment of DT gas fuelling and Ne seeding feedforward waveforms. However, it is difficult to avoid deep divertor detachment in the early L-mode phase after the H-L transition in case D1 (as indicated by a significantly widened low temperature region near the strike points up to 0.2 m from the separatrix shown in figure 28) even when the DT puff rate is also reduced to negligible levels. This is due to the slow reduction of the Ne particle content in the SOL during the transition, even if Ne seeding is completely switched off at the start of the transition (see figure 26). In these conditions, the Ne SOL content required to maintain the divertor power flux below 10 MWm^{-2} by Ne radiation can actually be sustained by the Ne core efflux that depletes the Ne core plasma level on a time scale $\tau_{\text{core Ne red.}} = \int n_{Ne} dV/\Gamma_{\text{pump, Ne}} \sim 40$ s. This large core efflux of Ne, combined with limited Ne pumping due

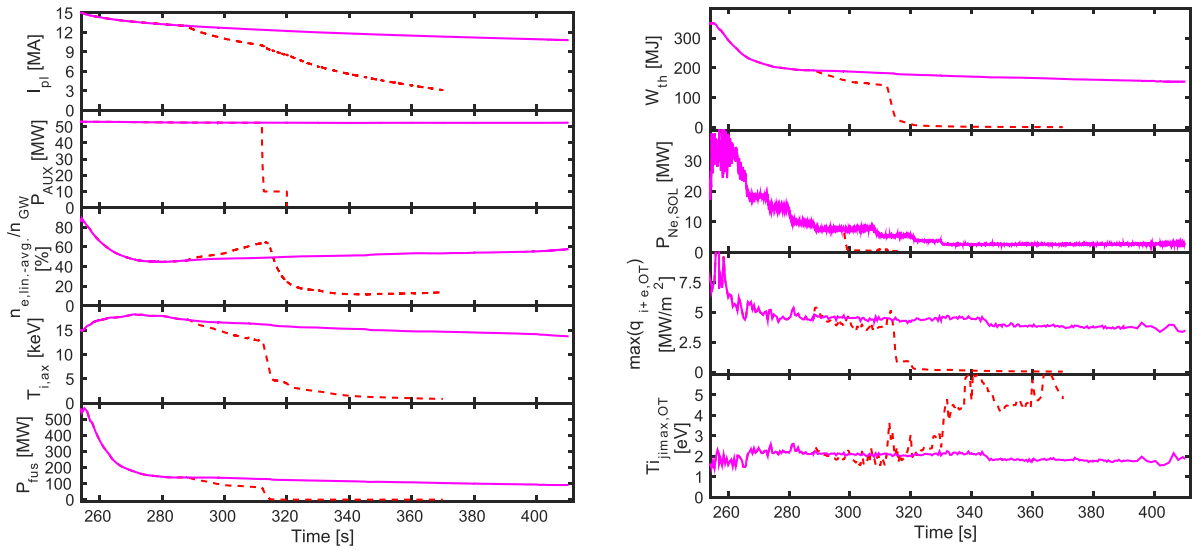

Figure 23. Left: time evolution of plasma current, auxiliary power, Greenwald density fraction, ion temperature on axis and fusion power, right: time evolution of the thermal core energy content, Ne induced radiation in the SOL and divertor plasma, the maximum power flux density at the outer target and ion temperature at the outer target location with the maximum absolute value of ion flux (from top to bottom), during current ramp-down in H-mode for cases C2b (magenta solid) and C2 (red dashed) discussed in the text.

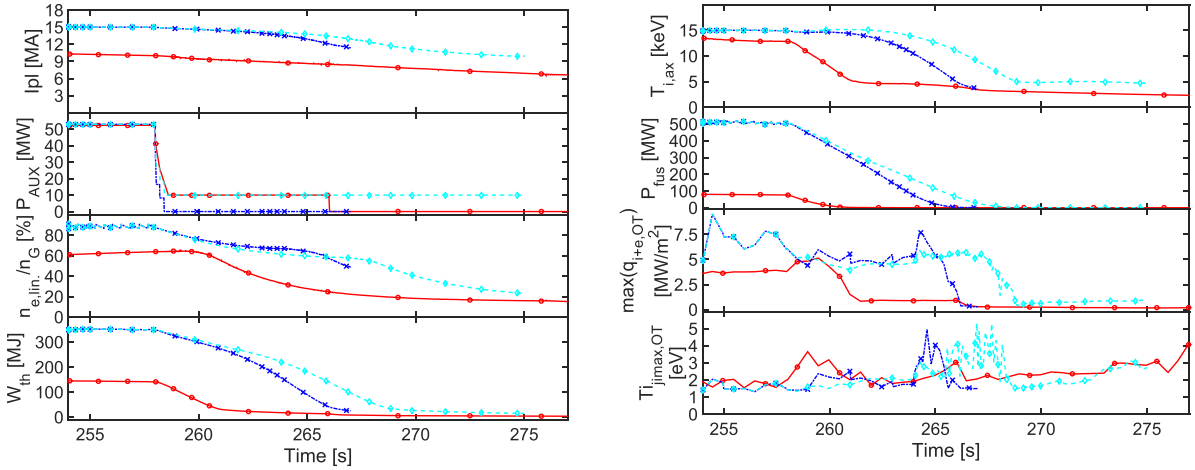

Figure 24. Left: time evolution of plasma current, auxiliary power, Greenwald density fraction, thermal core energy content, right: time evolution of ion temperature on axis, fusion power, the maximum power density at the outer target (considering power transferred by electrons, ions and due to recombination) and ion temperature at the outer target location with the maximum absolute value of ion flux (from top to bottom), for the refined calculation of the H-L transition phase during current ramp-down occurring at $I_{pl}\sim$15 MA (Case D1: blue crosses, Case D1b: cyan diamonds) and $I_{pl}\sim$10 MA (Case D2: red circles, shifted in time to match NB power switch off times).

to the low DT puffing, prevents the SOL Ne radiation to be reduced fast enough to avoid full detachment to set in in Case D1 (see figures 26 and 27), even though the relative importance of SOL Ne radiation may be diminished in these conditions due to a strong sensitivity of the Ne cooling rates in a low temperature environment (<∼30 eV). To avoid this situation and give sufficient time for Ne to be pumped out, 10 MW of ECRH power are maintained throughout the current ramp-down phase and this prevents divertor collapse and provides an edge-core integrated scenario (D1b) for the exit from high Q_{fus} at 15 MA and current ramp-down with realistic Ne pumping (see figures 24 and 28). In complementary simulations (not shown here), it has been confirmed that the Ne pumping efficiency can be increased by the application of higher DT gas puff rates in this phase. This increase is, however, limited as the applicable DT gas puff rates during the transition are limited to a few 10^{22} s^{-1} in the early phase of the transition and to only $\sim$1.0–1.5 $\cdot$ 10^{22} s^{-1} in the later phase to avoid the plasma density increasing and deep divertor detachment setting in.

For H-L transitions in the current ramp-down (case D2), the Ne control issues are much less severe. Already at the time of the H-L transition at $I_{pl}\sim$10 MA, the content of Ne in the SOL and divertor is negligible and divertor power fluxes and plasma temperature can be maintained below the required limits by DT fuelling alone (see figure 24, right, figure 26). For this reason, the problem with detachment in L-mode due to Ne contamination does not appear in the simulations of a late H-L transition.

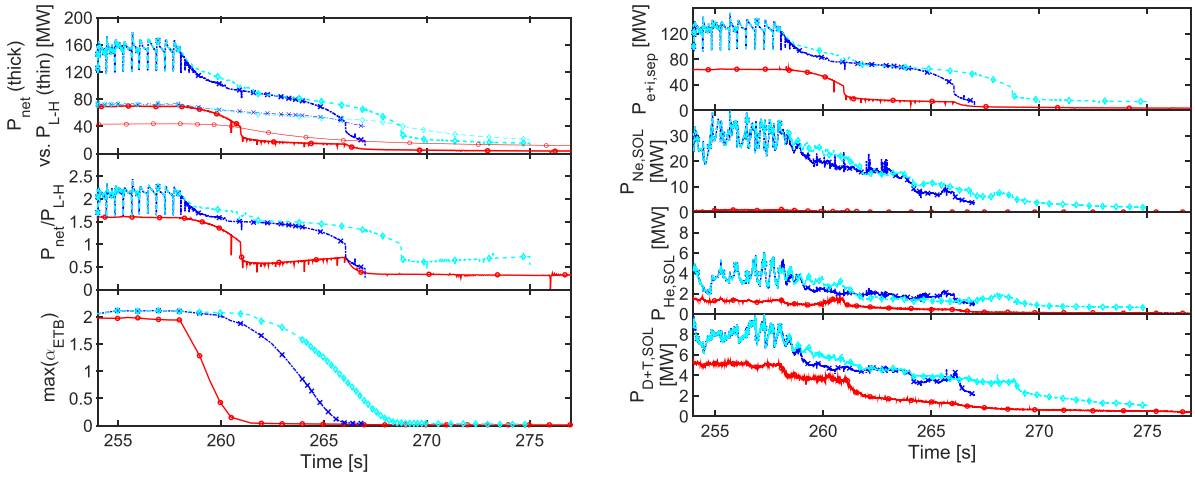

Figure 25. Left: time evolution of the net power (solid) vs. the L-H transition power threshold (dashed), the ratio between the net power and the L-H transition power threshold and the maximum normalised pressure gradient in the ETB, right: time evolution of the heat flux at the separatrix (i.e. P_{net}), the Ne, He and D + T induced radiation in the SOL and divertor (from top to bottom), for the refined calculation of the H-L transition phase during current ramp-down occurring at $I_{\mathrm{pl}}\sim$15 MA (Case D1: blue crosses, Case D1b: cyan diamonds) and $I_{\mathrm{pl}}\sim$10 MA (Case D2: red circles, shifted in time to match NB power switch off times).

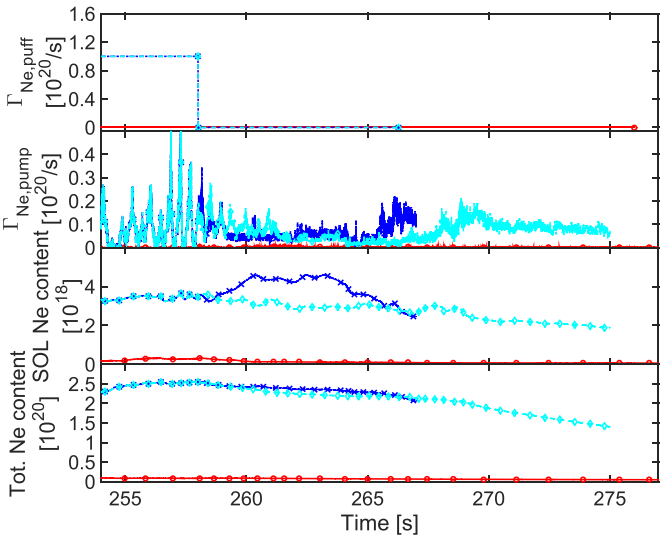

Figure 26. Time evolution of the Ne puff rate, the Ne pump rate, the Ne particle content in the SOL and the total Ne particle content in the core, SOL and divertor (from top to bottom), for the refined calculation of the H-L transition phase during current ramp-down occurring at $I_{\mathrm{pl}}\sim$15 MA (Case D1: blue crosses, Case D1b: cyan diamonds) and $I_{\mathrm{pl}}\sim$10 MA (Case 2: red circles, shifted in time to match NB power switch off times).

5. Summary

This paper presents coupled core + edge + SOL transport simulations (using JINTRAC) of the complete 15 MA 5.3 T DT ITER baseline scenario in the diverted phase, focussing on fuelling and impurity seeding requirements for core density and divertor heat load control in non-stationary phases.

As the main key result from this study, the JINTRAC simulations have demonstrated that viable ITER plasma scenarios can be realised, with the baseline fuelling capabilities (pellets, gas puff and impurity seeding) and heating and current drive schemes, to robustly access high Q_{fus} H-mode scenarios required to demonstrate $Q_{\mathrm{fus}} = 10$ with $\mathrm{P_{AUX}} \leq 53$ at 15 MA. Furthermore, our simulations show that a controlled back transition to L-mode and reduction in current to terminate the discharge is possible, while respecting all main operational constraints throughout the entire scenario. Complementary studies with JINTRAC-DINA IMAS have shown that these scenarios are within the capabilities of the ITER PF system [65]. The operational constraints considered in our studies can be summarised as follows:

- Constraints related to divertor control and particle throughput:
  - Maintenance of low ion temperatures < ∼5 eV near the strike point locations on both divertor targets for the avoidance of excessive W sputtering.

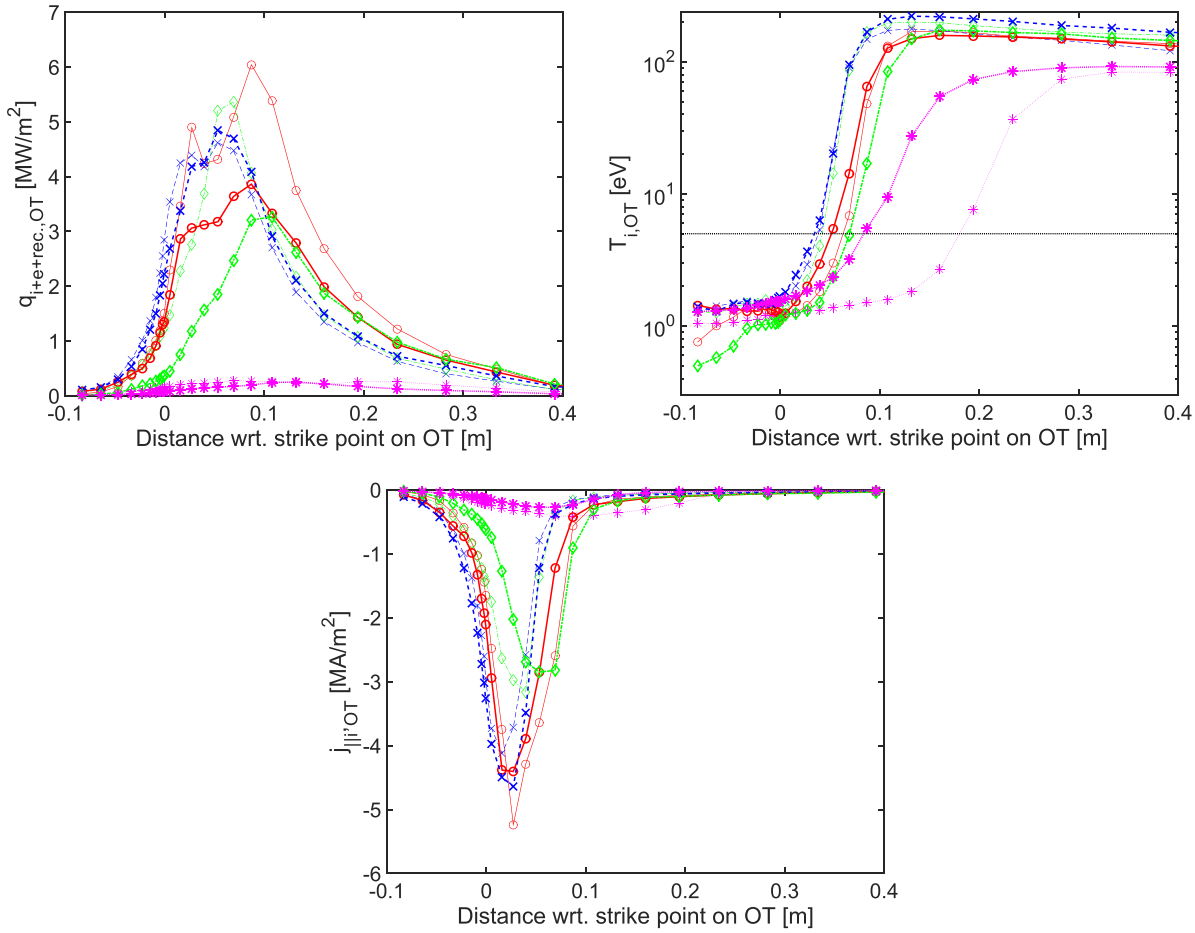

Figure 27. Profiles of power density (top left), ion temperature (top right) and the ion flux (bottom) at the outer target, for the refined calculation of the H-L transition phase during current ramp-down occurring at I_{pl}∼15 MA (Case D1, thin lines) and I_{pl}∼10 MA (thick lines) at several stages during and after the transition phase (red circles: start of transition, blue crosses: early ELM free H-mode phase, green diamonds: degraded H-mode before H-L transition, magenta stars: L-mode without auxiliary heat application). The heat flux is increased again at the time when the plasma is in a degraded H-mode regime for the H-L transition at I_{pl}∼15 MA, as the DT gas puff rate has been reduced to a very low level just before the H-L transition in order to reduce the risk of detachment after the H-L transition by excessive Ne radiation.

  - Maintenance of divertor heat loads below limit of ∼10 MWm^{-2}.
  - Avoidance of complete divertor detachment.
  - Application of a time-averaged total net particle throughput of < 200 Pa m^3 s^{-1}.
- Core density control:
  - Maintenance of core density below but (at high Q_{fus}) close to the Greenwald density limit.
  - Constraints on the density evolution after the L-H transition to ensure a robust access to a high density high Q_{fus} burning regime.
  - Upper limit in pedestal density to avoid core impurity accumulation via degradation of the temperature screening in the critical phases of the discharge.
- Constraints on P_{AUX}:
  - Available auxiliary EC power of 20 MW and NB power of 53 MW (additional 20 MW by IC are also available in ITER but have not been used in these simulations).
  - Satisfying the NB shine through limit ($P_{NB,shine\text{-}through}/P_{NB}$ < ∼5% [58]).
- Operational constraints imposed by PF coils and current control:
  - Upper limit in total poloidal flux consumption.
  - Maximum achievable current ramp rate.
  - Lower limit in plasma current for full bore plasma divertor configuration of ∼3 MA.

The simulations in this paper notably include all challenging transient phases in the diverted phase to address the critical core-edge integration issues. Our study is extensive but not exhaustive and has been focused on core-edge integration issues. Additional integration issues may need to be considered in the experiment to achieve a fully integrated scenario such as the control of sawteeth and NTMs [73] and ELM suppression/mitigation optimisation [39] which we have not considered. In addition, this study has not fully taken into account the time delays for key actuators (e.g. response times of a few hundred milliseconds for the gas injection system [63, 74]) in our feedback schemes. These can be addressed in future work via JINTRAC-IMAS simulations which can potentially

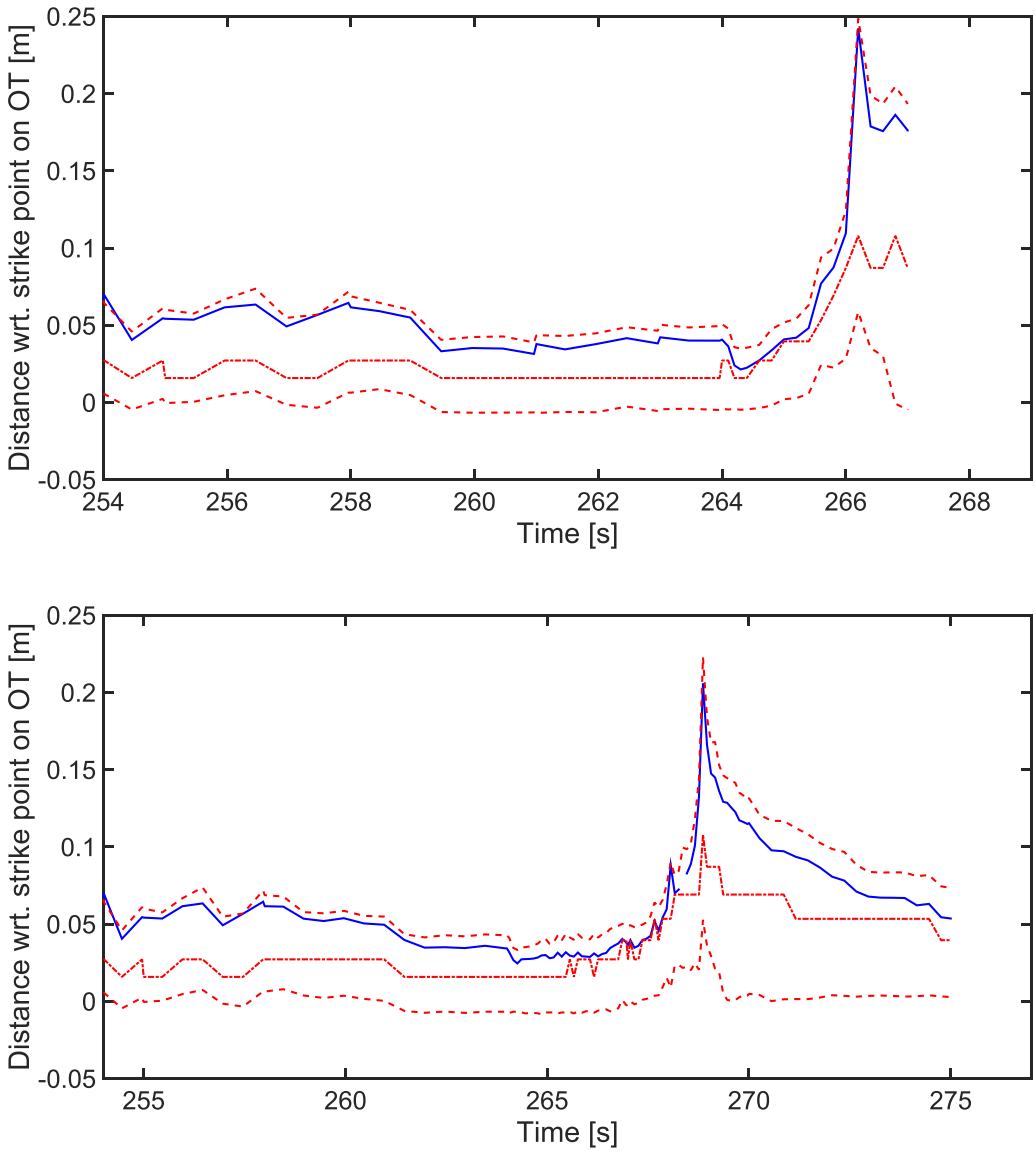

Figure 28. Time evolution of the locations on the outer divertor target where $T_i = 5$ eV (blue solid, lower T_i achieved at lower distance wrt. strike point location), where the maximum ion flux density is reached (red solid) and where half of the maximum ion flux density is obtained (red dashed) for the refined calculation of the H-L transition phase during current ramp-down occurring at Ipl∼15 MA (top: Case D1, bottom: Case D1b).

be coupled to the ITER Plasma Control System Simulation Platform (PCSSP).

The full plasma scenario simulations reported in this paper confirm several tentative findings from earlier modelling work, now with full edge-core modelling, relating to the optimisation of the core plasma, including: establishment of schemes for current ramp-up optimisation with respect to poloidal flux consumption and the safety factor at the start of flat-top [1, 35, 59]; the limitations in achievable density for purely gas fuelled plasmas [5]; the compatibility with PF coil current shape and stability control constraints [1]; the strategy for density ramp after L-H transition to high Q_{fus} at low $P_{sep}/P_{L\text{-}H}$ [18, 19]; the pellet fuelling requirements to achieve high density high Q_{fus} scenario [22, 29]; the challenge for divertor control due to pellet-induced perturbations [71]; and the fact that the H-L transition time exceeds the feedback reaction time for plasma position control and the plasma position thus can be controlled [1, 17].

The simulations presented here have also made a number of new findings. Firstly, during the L-mode I_{pl} ramp-up:

- The operational range in $n_{e,lin.\text{-}avg.}/n_{GW}$ is restricted to ∼20 ± 5% for P_{AUX}∼10–20 MW during ramp-up because of the simultaneous requirements: to keep $T_i < \sim 5$ eV near strike points to minimise W sputtering; keeping power flux densities on the target plates below 10 MWm^{-2} and keeping the SOL plasma stable by avoiding full divertor detachment.
- Pure Ohmic plasmas should be avoided during the I_{pl} ramp up because: high poloidal flux consumption would limit the maximum burn duration; with Ohmic heating alone the achievable $n_{e,lin.\text{-}avg.}/n_{GW}$ will be very low ($\lesssim$∼15%) so

that divertor power flux control is difficult when P_{AUX} is increased.

Secondly, the transition to high quality Q_{fus} H-mode may be more difficult if the L-H transition takes place at low I_{pl} during the ramp-up for the following reasons:

- If the I_{pl} ramp-up continues in H-mode, the current induced at the edge takes longer to diffuse to the core, and li(3) is likely to drop below the critical value for shape control [50]. Reducing the I_{pl} ramp-up rate to keep an acceptable li(3) would reduce the maximum burn duration. Furthermore, with our model of plasma transport we find that plasma transport is significantly degraded during the I_{pl} ramp-up, while s/q is reduced in the core [1].
- The achievable W_{th} in stationary H-mode is reduced after an H-mode transition at lower I_{pl} (e.g. 10 MA), the core T_i does not significantly exceed 10 keV (the critical temperature for the onset of fusion reactions and alpha heating), and it becomes more difficult to keep $P_{net} \gg P_{L\text{-}H}$. This extends the post-transition phase where divertor control may be more challenging, delays the post L-H density ramp, and reduces the maximum burn duration.
- Pellet injection is required after an early NB triggered L-H transition to keep the density above the NB shine-through limit, further complicating the transition to a high quality H-mode. The plasma stays closer to the L-H threshold, which increases the risk of failure to reach high Q_{fus}. In addition, the divertor is operated closer to full detachment after the L-H transition due to the wider fall-off length associated with high q plasmas. Due to increased divertor control challenges after an early L-H transition, small-size pellets need to be injected to increase the density while reducing the transient edge plasma perturbations triggered by pellets. As the pellet fuelling efficiency dominated by the diamagnetic inwards drift is reduced at lower plasma edge temperatures, the fuelling throughput required to support adequate core fuelling is significantly enhanced in this phase.

Thirdly, for L-H transitions in the I_{pl} flat-top, the transition to high quality high Q_{fus} H-mode is found to be easier to achieve, provided that, as described in [18, 19], the core density is increased slowly by pellet fuelling to ensure that the power near the separatrix stays well above $P_{L\text{-}H}$. Ne seeding is not required while the pedestal pressure has not yet approached the edge MHD limit, since the power flux at the targets can be maintained below 10 MWm^{-2} by only adjusting the D + T fuelling only. However, as soon as the pedestal pressure and the core energy content have approached the limit imposed by edge MHD and determined for the core transport model chosen, the power flux to the SOL increases on an energy confinement time scale. To accommodate this increase, significant Ne needs to be present in the SOL at this time to provide the necessary divertor radiation. The exact start time of the ELMy H-mode phase needs to be anticipated in order to start Ne seeding at the right time in order to provide the required level of SOL radiation when it is needed. Although we have obtained simulations that achieve the required goal, this critical phase of the scenario for the control of impurity radiation in the divertor warrants further dedicated follow-up studies including ITER-realistic time delays for the provision of Ne seeding to the plasma.

Finally, for the termination of the high Q_{fus} phase and current ramp-down, we find that having the H-L transition well into the I_{pl} ramp-down is very favourable from the point of view of divertor power flux and temperature control. At lower I_{pl} the P_{α} and dW_{th}/dt are lower and the divertor fall-off length is larger which leads to lower divertor power fluxes. These are found to be of a level that does not require Ne seeding for their control so that Ne can be pumped out of the plasma before the H-L transition takes place thus ensuring a thermally stable L-mode plasma. If the H-L transition is performed at higher currents and Ne still needs to be present at the time of the H-L transition, the control of the SOL Ne concentration in the follow-up L-mode phase is found to be challenging. To avoid full detachment in the follow-up L-mode phase, Ne would need to be removed from the SOL on short time scales. This is not possible with the baseline pumping in ITER because of the significant Ne outflux from the confined plasma into the SOL. In these cases it is necessary to maintain auxiliary heating at a level of ~10–20 MW during the L-mode phase to avoid complete plasma detachment triggered by the remnant Ne content in the SOL causing substantial divertor plasma cooling.

As a concluding remark, it is important to note that some of the quantitative aspects of the findings of the studies presented in this paper are sensitive to detailed modelling assumptions that will need to be refined in the future as progress is made in the understanding of the physics processes that dominate plasma transport in the core, edge transport barrier, SOL and divertor and their modelling. This being said, the qualitative plasma behaviour described by our modelling is based on robust physics assumptions and thus can be used to define the experimental strategies for the development of edge-core fully integrated ITER scenarios for the demonstration of the $Q_{fus} \sim 10$ goal.

Acknowledgments

This work was funded jointly by the RCUK Energy Programme (Grant No. EP/I501045) and ITER Task Agreement C19TD51FE (implemented by Fusion for Energy under Grant GRT-502). The views and opinions expressed do not necessarily reflect those of Fusion for Energy which is not liable for any use that may be made of the information contained herein. ITER is the Nuclear Facility INB No. 174. The views and opinions expressed herein do not necessarily reflect those of the ITER Organization. The authors are grateful to Dr. C. M. Roach, Dr. F. Casson, Dr. S. Henderson and the JINTRAC modelling and development team for useful consultations, helpful advice and support of our studies.

ORCID iDs

F. Koechl https://orcid.org/0000-0001-9706-6855
R. Ambrosino https://orcid.org/0000-0001-8799-5837

L. Garzotti https://orcid.org/0000-0002-3796-9814
A. Kukushkin https://orcid.org/0000-0001-6378-7128
M. Mattei https://orcid.org/0000-0001-7951-6584
E. Militello-Asp https://orcid.org/0000-0001-8183-8734
G. Saibene https://orcid.org/0000-0003-3597-9848

References

[1] Parail V. *et al* 2013 *Nucl. Fusion* **53** 113002
[2] Kessel C.E. *et al* 2015 *Nucl. Fusion* **55** 063038
[3] Kim S.H. *et al* 2018 *Nucl. Fusion* **58** 056013
[4] Kukushkin A.S. and Pacher H.D. 2002 *Plasma Phys. Control. Fusion* **44** 931–43
[5] Romanelli M. *et al* 2015 *Nucl. Fusion* **55** 093008
[6] Romanelli M. *et al* 2014 *Plasma Fusion Res.* **9** 3403023
[7] Cenacchi G. and Taroni A. 1988 JETTO: a free-boundary plasma transport code (basic version) JET Report JET-IR(88)03 JET Joint Undertaking
[8] Lauro-Taroni L. *et al* 1994 *Proc. 21st EPS Conf. on Controlled Fusion Plasma Physics* (Montpellier, France, 27 June–1 July 1994) vol 18B p 102 (http://euro-fusionscipub.org/archives/jet-archive/impurity-transport-of-high-performancedischarges-in-jet)
[9] Simonini R. *et al* 1994 *Contrib. Plasma Phys.* **34** 368
[10] Reiter D. 1992 *J. Nucl. Mater.* **196-198** 80–89
[11] Militello-Asp E. *et al* 2016 ITER fuelling requirements and scenario development for H, He and DT through JINTRAC integrated modelling *Preprint: 2016 IAEA Fusion Energy Conf.* (Kyoto, Japan, 17–22 October 2016) TH/P2-23 (https://nucleus.iaea.org/sites/fusionportal/Shared%20Documents/FEC%202016/fec2016-preprints/preprint0255.pdf)
[12] Kukushkin A.S. *et al* 2009 *Nucl. Fusion* **49** 075008
[13] Lipschultz B. *et al* 1984 *Nucl. Fusion* **24** 977
[14] Kallenbach A. *et al* 2015 *Nucl. Fusion* **55** 053026
[15] Belo P. *et al*, *Proc. 42nd EPS Conf. on Plasma Physics* (Lisbon, Portugal, 22–26 June 2015) P4.120 (http://ocs.ciemat.es/EPS2015PAP/pdf/P4.120.pdf)
[16] Garzotti L. *et al*, *Proc. 43rd EPS Conf. on Plasma Physics* (Leuven, Belgium, 4–8 July 2016) O4.113 (http://ocs.ciemat.es/EPS2016PAP/pdf/O4.113.pdf)
[17] Loarte A. *et al* 2014 *Nucl. Fusion* **54** 123014
[18] Loarte A. *et al* 2013 *Nucl. Fusion* **53** 083031
[19] Koechl F. *et al* 2017 *Nucl. Fusion* **57** 086023
[20] de Vries P.C. *et al* 2017 *Nucl. Fusion* **58** 026019
[21] Poli F.M. *et al* 2018 The plasma current ramp-down in ITER: physics constraints on control *Preprint: 2018 IAEA Fusion Energy Conf.* (Gandhinagar, India, 22–27 October 2018) EX/P7-27 (https://nucleus.iaea.org/sites/fusionportal/Shared%20Documents/FEC%202018/fec2018-preprints/preprint0295.pdf)
[22] Garzotti L. *et al* 2019 *Nucl. Fusion* **59** 026006
[23] Koechl F. *et al* 2018 *Plasma Phys. Control. Fusion* **60** 074008
[24] Fichtmüller M. *et al* 1998 *Czech. J. Phys.* **48** 25–38
[25] Houlberg W.A. *et al* 1997 *Phys. Plasmas* **4** 3230
[26] Summers H.P. *et al* 2007 *AIP Conf. Proc.* **901** 239
[27] Erba M. *et al* 1997 *Plasma Phys. Control. Fusion* **39** 261–76
[28] Waltz R.E. *et al* 1997 *Phys. Plasmas* **4** 2482
[29] Garzotti L. *et al* 2012 *Nucl. Fusion* **52** 013002
[30] Erba M. *et al* 1996 Validation of a new mixed Bohm/gyro-bohm transport model on discharges of the ITER Data-base JET Report JET-R(96)07 (http://euro-fusionscipub.org/archives/jet-archive/validation-of-a-new-mixed-bohmgyro-bohmtransport-model-on-discharges-of-the-iter-data-base)
[31] Bizarro J.P.S. *et al* 2016 *Plasma Phys. Control. Fusion* **58** 105010
[32] Summers H.P. 2001 The ADAS manual version 2.3 (http://adas.ac.uk)
[33] Sartori R. 2004 *Plasma Phys. Control. Fusion* **46** 723
[34] Martin Y.R. *et al* 2008 *J. Phys.: Conf. Ser.* **123** 012033
[35] Parail V. *et al* 2009 *Nucl. Fusion* **49** 075030
[36] Snyder P. *et al* 2009 *Phys. Plasmas* **16** 056118
[37] Polevoi A.R. *et al* 2015 *Nucl. Fusion* **55** 063019
[38] Loarte A. *et al* 2018 Advances in modelling of plasma pedestal behaviour and ELM control in ITER reference plasma scenarios *Preprint: 2018 IAEA Fusion Energy Conf.* (Gandhinagar, India, 22–27 October 2018) EX/P7-23 (https://nucleus.iaea.org/sites/fusionportal/Shared%20Documents/FEC%202018/fec2018-preprints/preprint0482.pdf)
[39] Loarte A. *et al* 2014 *Nucl. Fusion* **54** 033007
[40] Futatani S. *et al* 2016 Non-linear MHD simulations of pellet triggered ELMs *Preprint: 2016 IAEA Fusion Energy Conf.* (Kyoto, Japan, 17–22 October 2016) TH/P1-25 (https://nucleus.iaea.org/sites/fusionportal/Shared%20Documents/FEC%202016/fec2016-preprints/preprint0186.pdf)
[41] Challis C.D. *et al* 1989 *Nucl. Fusion* **29** 563
[42] Heikkinen J.A. *et al* 1995 *Phys. Plasmas* **2** 3724
[43] Hirvijoki E. *et al* 2014 *Comput. Phys. Commun.* **185** 1310–21
[44] Farina D. 2007 *Fusion Sci. Technol.* **52** 154
[45] Brezinsek S. *et al* 2013 *Nucl. Fusion* **53** 083023
[46] Pégourié B. *et al* 2005 *Plasma Phys. Control. Fusion* **47** 17–35
[47] Pégourié B. *et al* 2007 *Nucl. Fusion* **47** 44–56
[48] Polevoi A.R. *et al* 2017 *Nucl. Fusion* **57** 022014
[49] Albanese R., Mattei M. and Villone F. 2004 *Nucl. Fusion* **44** 999
[50] Mattei M. *et al* 2009 *Fusion Eng. Des.* **84** 300–4
[51] Braginski V.I. 1965 *Review of Plasma Physics* ed M.A. Leontovich (New York: Consultants Bureau)
[52] Cohen R.H. *et al* 1994 *Contrib. Plasma Phys.* **34** 198
[53] Krasheninnikov S. *et al* 1994 *Contrib. Plasma Phys.* **34** 151
[54] Radford G.J. *et al* 1992 *Contrib. Plasma Phys.* **32** 297
[55] Wiesen S. *et al* 2011 *Plasma Phys. Control. Fusion* **53** 124039
[56] Kukushkin A.S. *et al* 2013 *J. Nucl. Mater.* **438** S203
[57] Pacher H.D. *et al* 2015 *J. Nucl. Mater.* **463** 591–5
[58] Singh M.J. *et al* 2017 *New J. Phys.* **19** 055004
[59] Imbeaux F. *et al* 2011 *Nucl. Fusion* **51** 083026
[60] Gribov Y. *et al* 2015 *Nucl. Fusion* **55** 073021
[61] Hogeweij G.M.D. *et al* 2013 *Nucl. Fusion* **53** 013008
[62] Dux R. *et al* 2014 *Plasma Phys. Control. Fusion* **56** 124003
[63] Bonnin X. *et al* 2017 *Nucl. Mater. Energy* **12** 1100
[64] Citrin J. *et al* 2012 *Plasma Phys. Control. Fusion* **54** 065008
[65] Koechl F. *et al* 2018 Optimising the ITER 15 MA DT baseline scenario by exploiting a self-consistent free-boundary core-edge-SOL workflow in IMAS *Preprint: 2018 IAEA Fusion Energy Conf.* (Gandhinagar, India, 22–27 October 2018) EX/P7-25 (https://nucleus.iaea.org/sites/fusionportal/Shared%20Documents/FEC%202018/fec2018-preprints/preprint0593.pdf)
[66] Polevoi A.R. *et al* 2013 *Nucl. Fusion* **53** 123026
[67] Maget P. *et al* 2013 *Nucl. Fusion* **53** 093011
[68] Baylor L. *et al* 2015 *Proc. IEEE 26th Symp. on Fusion Engineering* (Austin, TX, 31 May–4 June 2015) SO18-3 (https://ieeexplore.ieee.org/stamp/stamp.jsp?tp=&arnumber=7482362)
[69] Eich T. *et al* 2013 *Nucl. Fusion* **53** 093031
[70] Chang C.S. *et al* 2017 *Nucl. Fusion* **57** 116023
[71] Wiesen S. *et al* 2017 *Nucl. Fusion* **57** 076020
[72] Koechl F. *et al* 2012 *Proc. 39th EPS Conf. on Plasma Physics* (Stockholm, Sweden, 2–6 July 2012) P1.042 (http://ocs.ciemat.es/EPSICPP2012PAP/pdf/P1.042.pdf)
[73] Poli F.M. *et al* 2018 *Nucl. Fusion* **58** 016007
[74] Snipes J.A. *et al* 2017 *Nucl. Fusion* **57** 125001